to appear in the Journal of Computational Physics

Discrete-velocity models and numerical schemes for the Boltzmann-BGK equation in plane and axisymmetric geometries

Luc Mieussens

Mathématiques Appliquées de Bordeaux,
Université Bordeaux I, 351 Cours de la Libération,
33405 Talence Cedex, France

E-mail: Luc.Mieussens@math.u-bordeaux.fr

We present new numerical models for computing transitional or rarefied gas flows as described by the Boltzmann-BGK and BGK-ES equations. We first propose a new discrete-velocity model, based on the entropy minimization principle. This model satisfies the conservation laws and the entropy dissipation. Moreover, the problem of conservation and entropy for axisymmetric flows is investigated. We find algebraic relations that must be satisfied by the discretization of the velocity derivative appearing in the transport operator. Then we propose some models that satisfy these constraints. Owing to these properties, we obtain numerical schemes that are economic, in terms of discretization, and robust. In particular, we develop a linearized implicit scheme for computing stationary solutions of the discrete-velocity BGK and BGK-ES models. This scheme is the basis of a code which can compute high altitude hypersonic flows, in 2D plane and axisymmetric geometries. Our results are analyzed and compared to other methods.

Key Words: Boltzmann equation; BGK model; discrete-velocity models; axisymmetric flows; implicit schemes; conservative and entropic methods

1. INTRODUCTION

For the simulation of gas flows in rarefied or transitional regimes, there mainly exists two classes of methods. The first one is a probabilistic approach, like the classical Direct Simulation Monte Carlo method (DSMC). The second approach is called deterministic. It consists in numerically solving the kinetic equation, namely the Boltzmann equation.

The DSMC method is the most often used in engineering applications. But due to its particular nature, this method is still expensive for some flows like recirculation problems or near continuum flows. However, it is worth mentioning the recent

approach of Pareschi and Caflisch [28] that proposes a modification of DSMC to correct this problem. But the probabilistic nature of DSMC also leads to noise charged solutions. The deterministic approaches are more accurate (see Rogier-Schneider [30], Buet [11], Ohwada [27]), but they are very expensive in terms of computational time, especially due to to the quadratic cost of the velocity discretization of the collision operator.

A reduction of this cost can be obtained by considering simplified models of the Boltzmann equation, like the Bathnagar-Gross-Krook model (BGK)

$$\partial_t f + v \cdot \nabla_{\mathrm{x}} f = \frac{1}{\tau}(M[f] - f).$$

This model [5] is known to be sufficient for numerous situations, even in some cases where the gas is far from equilibrium (see [18]). Some drawbacks of this model as the incorrect value of the Prandtl number can be corrected by modified models. A lot of works have been devoted to numerical approximations of the BGK equation, essentially by the discrete-ordinate method (see Yang and Huang in [36] and Aoki, Kanba and Takata in [3] and their references), but also by particular methods (see Issautier in [20]). However, to our knowledge, none of these methods satisfy at the discrete level the macroscopic properties known as conservation laws and dissipation of entropy.

In this work, we are essentially concerned by developing numerical methods that are conservative and entropic. For that reason, this paper presents three distinct points. First we present a robust velocity discretization of the BGK and BGK-Ellipsoidal-Statistical (BGK-ES) collision operators. Then the velocity discretization of the transport operator is considered, especially for cylindrical coordinates. These two points give us discrete-velocity models of BGK and BGK-ES equations, that are discretized in space and time in the last point.

For the velocity discretization of the BGK collision operator, the main problem is the approximation of the Maxwellian distribution. Many works use precise quadratures of Gauss-Hermite type (see [36, 3]). But despite the accuracy of their quadratures, these methods lack the properties of conservation and dissipation of entropy. This makes necessary a fine velocity mesh to ensure robust algorithms, which then are expensive. We have proposed in [26] a method based on an entropy minimization principle, which gives a conservative and entropic discrete BGK collision operator. Here, we advance the work of [26] and generalize the method to the BGK-ES operator. This allows us to reach correct Prandtl number in the hydrodynamic limit.

The velocity discretization of the transport operator is trivial in Cartesian coordinates, but not in cylindrical coordinates. In fact, the cylindrical description yields inertia terms that are velocity derivatives of the distribution function. This problem is important to simulate axisymmetric flows, but to our knowledge, a few articles exist about the numerical approximation of this operator. One of the first work is due to Bergers in [6] (see also his references). He approximates the inertia terms by assuming that they are equal to that given by a Maxwellian distribution. However this assumption is not valid for strong kinetic non equilibrium, as with strong shock waves normal to the radial direction. In the works of Shakhov [31], Sone et al. [35], and Larina and Rykov [22], the inertia terms are directly discretized, but one or all

the properties of positivity, conservation, and entropy are lost. Consequently, these methods may lack robustness and are restricted to simple 1D or 2D axisymmetric flows like in circular pipes or between two coaxial cylinders.

Here we follow the same velocity discretization approach of the previous authors but we put in evidence the properties that should be satisfied by the discrete inertia terms so as to ensure conservation and entropy. We propose some corrections to existing methods to make them conservative. We also propose new discretizations that satisfy positivity of solution, conservation and entropy. To our knowledge, it is the first time that discretizations simultaneously possessing all these properties are presented. Moreover, we point out that these discretizations of the transport equation are independent of the collision term. Therefore they may be applied to a large class of kinetic equations as Boltzmann or Fokker-Planck equations.

The velocity discretization of the collision and transport operator leads to a so-called discrete-velocity model (DVM). This DVM must be discretized in space and time. First, we present an explicit scheme that inherits all the properties of the discrete-velocity model. However, in view of steady computations, the CFL condition of this scheme is restrictive in dense regimes (where τ is small) and in high-velocity regimes. To overcome this difficulty, there exists three different ways. First, many authors directly use a discretization of the stationary equation with fixed point techniques (see [3] and Babovski [4]). The drawback is that this method may converge very slowly (see a comparison in [26]). Another approach, quite recent, consists in developing schemes that are robust in the fluid dynamic limit (see Jin-Levermore [21], Gabetta-Pareschi-Toscani in [17], Caflisch et al. in [12]). But the problem of high velocity regimes does not seem to be resolved by these methods.

Our approach is a classical CFD technique which consists in developing a fully linearized implicit scheme, thus stable for any arbitrary relaxation time and any large velocity. A similar technique has been used by Yang and Huang [36], but in their work, only the negative term $-f$ of the collision operator is implicit. Our method involves solving a very large linear system, for which we propose an iterative solver. We use the sparse structure of the different matrices involved in the system, related to the different role of space and velocity variables. Our solver is then a kind of coupling between Jacobi and Gauss-Seidel methods. Our linearized implicit scheme appears to be very fast and robust for computing steady flows, for both dense and high speed regimes. We also present an adaptation of this scheme to curvilinear meshes and axisymmetric flows.

The remainder of the paper follows logically. In the next section, some properties of the BGK and BGK-ES equations are recalled, as well as a short list of notations. In section 3, we present our velocity discretization of the BGK and BGK-ES collision operators. In section 4, we discuss the problem of the velocity discretization of the transport operator in cylindrical coordinates. Then in section 5, we present our numerical schemes for discretizing in space and time our DVM. The linearized implicit scheme is derived from the explicit scheme and the linear solver algorithm is precisely described. The extension to axisymmetric DVM is also presented. Finally, the last section shows numerous numerical results for subsonic, supersonic, and hypersonic flows. Both plane and axisymmetric cases are presented. Plane flow computations show the difference between BGK and BGK-ES, the advantage

of our approach in comparison with classical DSMC computations for recirculation problems, and the ability of our method for computing hypersonic flows. For axisymmetric flows, the different velocity discretizations are compared on a simple 1D case, and the potentiality of our method is demonstrated on a 2D flow around a sphere. Whenever it is possible, our results are compared to DSMC and Navier-Stokes computations.

2. BGK EQUATION

The BGK equation is a simplified model of the Boltzmann equation [13] for rarefied gases, which describes the evolution of the mass density $f(t, \mathrm{x}, v)$ of monoatomic molecules that have position $\mathrm{x} = (x, y, z)$ and velocity $v = (v_x, v_y, v_z) \in \mathbf{R}^3$

$$\partial_t f + v \cdot \nabla_{\mathrm{x}} f = \frac{1}{\tau}(M[f] - f). \tag{1}$$

The collisions are modeled here by the relaxation of f towards the Maxwellian equilibrium distribution $M[f]$ (cf. [5]). This distribution only depends on v and on the fluid quantities - density ρ, mean velocity $u = (u_x, u_y, u_z)$ and temperature T - that are defined by the first five moments of f

$$\rho = \langle f \rangle, \qquad \rho u = \langle v f \rangle, \qquad E = \langle \tfrac{1}{2}|v|^2 f \rangle = \tfrac{1}{2}\rho|u|^2 + \tfrac{3}{2}\rho RT,$$

where $\langle g \rangle = \int g(v)\, dv$ denotes the integral of any vectorial or scalar function g. These moments are called density, momentum, and total energy of the gas. We denote by $\boldsymbol{m}(v) = (1, v, \frac{1}{2}|v|^2)^T$ the vector of microscopic quantities mass, momentum and kinetic energy (normalized by the mass). Similarly we denote by $\boldsymbol{\rho} = (\rho, \rho u, E)^T$ the vector of first five moments of f. These notations yield a more compact definition of the moments

$$\boldsymbol{\rho} = \langle \boldsymbol{m} f \rangle.$$

Note that throughout this paper, bold symbols are only used for vectors of $\mathbf{R}^5$ such as, for example, $\boldsymbol{\rho}$ and $\boldsymbol{m}(v)$. Since $M[f]$ depends only on $\boldsymbol{\rho}$, it will be denoted by $M[\boldsymbol{\rho}]$ in the sequel. An expression of $M[\boldsymbol{\rho}]$ is

$$M[\boldsymbol{\rho}] = \exp(\boldsymbol{\alpha} \cdot \boldsymbol{m}(v)), \quad \text{with } \boldsymbol{\alpha} = \left(\log\left(\frac{\rho}{(2\pi RT)^{3/2}} \right) - \frac{|u|^2}{2RT}, \frac{u}{RT}, -\frac{1}{RT} \right)^T \tag{2}$$

By definition, $M[\boldsymbol{\rho}]$ has the same moments as f and it can easily be seen that this distribution is the unique solution of the following entropy minimization problem (see for instance [29])

$$(\mathcal{P}) \qquad H(M[\boldsymbol{\rho}]) = \min \{ H(g),\ g \geq 0 \ s.t. \ \langle \boldsymbol{m} g \rangle = \boldsymbol{\rho} \}, \tag{3}$$

where $H(g) = \langle g \log g \rangle$ is the kinetic entropy of the distribution g. This simply means that the local equilibrium state minimizes the entropy of all the possible states leading to the same macroscopic properties.

With this characterization of the local Maxwellian equilibrium, the following properties of conservation of density, momentum, energy, and dissipation of entropy

may easily be proved

$$\partial_t \langle \boldsymbol{m} f \rangle + \nabla_{\mathrm{x}} \langle \boldsymbol{m} v f \rangle = 0, \tag{4}$$

$$\partial_t \langle f \log f \rangle + \nabla_{\mathrm{x}} \langle v f \log f \rangle \leq 0. \tag{5}$$

Furthermore, it is possible to check that solutions of (1) are nonnegative. We point out that in a numerical scheme, the preservation of these properties is essential to a robust and economic discretization.

The relaxation time of the BGK model is defined by

$$\tau^{-1} = c\rho T^{1-\delta}, \tag{6}$$

where δ is the exponent of the viscosity law of the gas (see [14]). It depends on the molecular interaction potential and on the type of the gas. The constant c is $RT^{\delta}_{ref}/\mu_{ref}$, where μ_{ref} is the viscosity of the gas at the reference temperature T_{ref}. We refer to a table in [7] for some values of δ and μ_{ref} of different gases.

The problem of this single relaxation time in the BGK model is that the collision operator leads to unrealistic values of the transport coefficients at the hydrodynamic limit. In particular, the Prandtl number Pr is then equal to 1, instead of the value $\frac{2}{3}$ given by both experimental data and a Chapman-Enskog expansion of the Boltzmann equation for monoatomic gases. There exist several BGK-like relaxation models that fit the correct Prandtl number (see the models of Shakhov [32], Liu [24], Holway [19], Bouchut-Perthame [9], Struchtrup [34]). However, a few models respect each constraints of positivity, conservation of moments, dissipation of entropy, as well as a low computational cost. Here, we consider the BGK-ES model introduced by Holway [19] where the collision operator is now

$$C(f) = \frac{1}{\tau}(G[f] - f).$$

In this model, the Maxwellian equilibrium is replaced by an anisotropic Gaussian $G[f]$ defined by

$$G[f] = \frac{\rho}{\sqrt{\det(2\pi\mathcal{T})}} \exp\left(-\tfrac{1}{2}(v-u)^T \mathcal{T}^{-1}(v-u)\right),$$

where $\rho\mathcal{T} = \frac{1}{Pr}\rho RTI + (1-\frac{1}{Pr})\rho\Theta$ is a linear combination of the stress tensor $\rho\Theta = \langle (v-u)\otimes(v-u) f\rangle$ and of the Maxwellian isotropic stress tensor $\rho RTI = \langle (v-u)\otimes(v-u) M[\boldsymbol{\rho}]\rangle$. The relaxation time is now defined by $\tau^{-1} = \frac{1}{Pr} c\rho T^{1-\delta}$. The Gaussian satisfies the following properties

$$\langle \boldsymbol{m} G[f]\rangle = \langle \boldsymbol{m} f\rangle, \qquad \langle (v-u)\otimes(v-u) G[f]\rangle = \rho\mathcal{T}, \tag{7}$$

$$H(G[f]) = \min\{H(g),\ g\geq 0,\ \langle (1, v, v\otimes v)^T g\rangle = (\rho, \rho u, \rho u\otimes u + \rho\mathcal{T})^T\}. \tag{8}$$

The model is thus positive and conservative, and the entropy dissipation property (H-theorem) has recently been proved by Andriès-Le Tallec-Perthame [2]. Also note that the fundamental equilibrium property

$$C(f) = 0 \Leftrightarrow f = M[\boldsymbol{\rho}]$$

is well satisfied. In fact $C(f) = 0$ implies $G[f] = f$, thus $\Theta = \frac{1}{Pr} RTI + (1 - \frac{1}{Pr})\Theta$. Consequently, $\Theta = RTI$ and therefore $f = G[f] = M[\boldsymbol{\rho}]$.

Owing to the structure of the BGK-ES operator, which is very close to that of the BGK operator, our numerical algorithms will be quite similar.

In this paper, the diffuse reflection is used for all gas-surface interactions. Incident molecules are assumed to be absorbed by the wall, and re-emitted with the temperature T_w of the wall and with a random velocity, according to a Maxwellian distribution centered on the velocity of the wall u_w:

$$f(t, \mathrm{x}, v) = \phi(\mathrm{x}) M[\boldsymbol{\rho}_w](v), \quad v \cdot n(\mathrm{x}) > 0, \tag{9}$$

where $\boldsymbol{\rho}_w = (1, u_w, \frac{1}{2}|u_w|^2 + \frac{3}{2}RT_w)$, $n(\mathrm{x})$ is the vector normal to the wall (directed toward the gas), and $\phi(\mathrm{x})$ is a parameter such that the mass flux across the wall is zero

$$\phi(\mathrm{x}) = -\frac{\int_{v\cdot n(\mathrm{x})<0} v \cdot n(\mathrm{x}) f(t, \mathrm{x}, v)\, dv}{\int_{v\cdot n(\mathrm{x})>0} v \cdot n(\mathrm{x}) M[\boldsymbol{\rho}_w](v)\, dv}.$$

We refer to [13] for a more detailed presentation of this reflection.

3. CONSERVATIVE AND ENTROPIC VELOCITY DISCRETIZATION OF THE COLLISION OPERATOR

Let $\mathcal{K}$ be a set of N_v multi-indexes of $\mathbf{Z}^3$, and let $\mathcal{V}$ be a discrete-velocity grid of N_v points $v_\mathrm{k} \in \mathbf{R}^3$ indexed by $\mathrm{k} = (k, l, q) \in \mathcal{K}$, and defined by

$$v_\mathrm{k} = (v_x^k, v_y^l, v_z^q) = (k\Delta v_x, l\Delta v_y, q\Delta v_z),$$

where $(\Delta v_x, \Delta v_y, \Delta v_z)$ are three positive numbers. The "continuous" velocity distribution f is then replaced by a N_v-vector $f_\mathcal{K}(t, \mathrm{x}) = (f_\mathrm{k}(t, \mathrm{x}))_{\mathrm{k}\in\mathcal{K}}$ where each component $f_\mathrm{k}(t, \mathrm{x})$ is assumed to be an approximation of $f(t, \mathrm{x}, v_\mathrm{k})$. These components will sometimes be denoted by $f_{k,l,q}(t, x)$. The fluid quantities are thus given as in continuous case, except that integrals on $\mathbf{R}^3$ are replaced by discrete sums on $\mathcal{V}$. That is, setting

$$\langle g \rangle_\mathcal{K} = \sum_{\mathrm{k}\in\mathcal{K}} g_\mathrm{k} \Delta v_x \Delta v_y \Delta v_z$$

for any vector $g \in \mathbf{R}^{N_v}$, we can define discrete moments and discrete entropy of $f_\mathcal{K}$ by

$$\begin{aligned} \boldsymbol{\rho}_\mathcal{K} &= \langle \boldsymbol{m} f_\mathcal{K} \rangle_\mathcal{K} = \sum_{\mathrm{k}\in\mathcal{K}} \boldsymbol{m}(v_\mathrm{k}) f_\mathrm{k} \Delta v_x \Delta v_y \Delta v_z, \\ H_\mathcal{K}(f_\mathcal{K}) &= \langle f_\mathcal{K} \log f_\mathcal{K} \rangle_\mathcal{K}. \end{aligned}$$

Our discrete velocity BGK model follows as a set of N_v equations

$$\partial_t f_\mathrm{k} + v_\mathrm{k} \cdot \nabla_\mathrm{x} f_\mathrm{k} = \frac{1}{\tau} \left(\mathcal{E}_\mathrm{k}[\boldsymbol{\rho}_\mathcal{K}] - f_\mathrm{k} \right), \qquad \forall \mathrm{k} \in \mathcal{K} \tag{10}$$

and the main problem is to define an approximation $\mathcal{E}_\mathcal{K}[\boldsymbol{\rho}_\mathcal{K}]$ of the Maxwellian equilibrium $M[\boldsymbol{\rho}]$ such that conservation properties (4) and entropy property (5)

still hold. First we note that the natural approximation (used by Yang and Huang in [36])

$$\mathcal{E}_{\mathrm{k}}[\boldsymbol{\rho}_{\mathcal{K}}] = M[\boldsymbol{\rho}_{\mathcal{K}}](v_{\mathrm{k}}), \qquad \forall \mathrm{k} \in \mathcal{K}, \tag{11}$$

cannot satisfy these requirements. Instead, we propose to use the discrete version of entropy minimization problem (3). Let $\mathcal{E}_{\mathcal{K}}[\boldsymbol{\rho}_{\mathcal{K}}]$ be defined by the minimum of discrete entropy, with the constraints that it must have the same moments as $f_{\mathcal{K}}$, *i.e.* $\mathcal{E}_{\mathcal{K}}[\boldsymbol{\rho}_{\mathcal{K}}]$ is the solution of the following problem

$$(\mathcal{P}_{\mathcal{K}}) \qquad H_{\mathcal{K}}(\mathcal{E}_{\mathcal{K}}[\boldsymbol{\rho}_{\mathcal{K}}]) = \min\left\{H_{\mathcal{K}}(g),\ g \geq 0 \in \mathbf{R}^{N_v}\ s.t.\ \langle \boldsymbol{m} g\rangle_{\mathcal{K}} = \boldsymbol{\rho}_{\mathcal{K}}\right\}.$$

Obviously, it must be checked that this problem has a unique and easily solvable solution (solving directly $(\mathcal{P}_{\mathcal{K}})$ in $\mathbf{R}^{N_v}$ would be numerically expensive). In the continuous case, the condition $\rho, T > 0$ is sufficient to characterize the solution of (3) by the Maxwellian distribution. However, this is not true for the discrete case where explicit computations are not possible. To this end, we have then proved in [15, 26] that under a natural assumption on $\mathcal{V}$, the discrete equilibrium $\mathcal{E}_{\mathcal{K}}[\boldsymbol{\rho}_{\mathcal{K}}]$ has an exponential form *if, and only if,* a "strict realizability" condition is fulfilled by $\boldsymbol{\rho}_{\mathcal{K}}$:

THEOREM 3.1. *Let $\boldsymbol{\rho}_{\mathcal{K}}$ be a vector in $\mathbf{R}^5$, such that the set $\mathcal{X}_{\boldsymbol{\rho}_{\mathcal{K}}} = \{g \geq 0 \in \mathbf{R}^{N_v}\ s.t.\ \langle \boldsymbol{m} g\rangle_{\mathcal{K}} = \boldsymbol{\rho}_{\mathcal{K}}\}$ of nonnegative discrete distributions realizing $\boldsymbol{\rho}_{\mathcal{K}}$ is not empty. Then, the problem $(\mathcal{P}_{\mathcal{K}})$ has a unique solution $\mathcal{E}_{\mathcal{K}}[\boldsymbol{\rho}_{\mathcal{K}}]$ called discrete equilibrium. Moreover, we assume that $\mathcal{V}$ has at least three points in each direction. Then there exists a unique vector $\boldsymbol{\alpha}$ in $\mathbf{R}^5$ such that the following exponential characterization holds*

$$\mathcal{E}_{\mathrm{k}}[\boldsymbol{\rho}_{\mathcal{K}}] = \exp(\boldsymbol{\alpha} \cdot \boldsymbol{m}(v_{\mathrm{k}})), \qquad \forall \mathrm{k} \in \mathcal{K},$$

if and only if $\boldsymbol{\rho}_{\mathcal{K}}$ is strictly realizable, i.e.

$$\exists g \in \mathcal{X}_{\boldsymbol{\rho}_{\mathcal{K}}}\ s.t.\ g > 0. \tag{12}$$

REMARK 3.1. *Due to the above result, the computation of $\mathcal{E}_{\mathcal{K}}[\boldsymbol{\rho}_{\mathcal{K}}]$ does not require the solution of an expensive minimization problem in $\mathbf{R}^{N_v}$. Instead, only the computation of the vector $\boldsymbol{\alpha}$ in $\mathbf{R}^5$ is necessary. This vector $\boldsymbol{\alpha}$ is the unique solution of the nonlinear set of five equations*

$$\langle \boldsymbol{m} \exp(\boldsymbol{\alpha} \cdot \boldsymbol{m})\rangle_{\mathcal{K}} = \boldsymbol{\rho}_{\mathcal{K}},$$

since $\mathcal{E}_{\mathcal{K}}[\boldsymbol{\rho}_{\mathcal{K}}]$ realizes $\boldsymbol{\rho}_{\mathcal{K}}$. This set may be solved by a Newton algorithm (see Sec.5). Note that for plane flows, we have $u_z = 0$. Then this set reduces to four equations only, and we set $\boldsymbol{m}(v) = (1, v_x, v_y, \frac{1}{2}|v|^2)$ and $\boldsymbol{\rho} = (\rho, \rho u_x, \rho u_y, E)$.

REMARK 3.2. *Note that the case where $\mathcal{X}_{\boldsymbol{\rho}_\mathcal{K}}$ is empty is not considered here, since the model implicitly contains the fact that $\boldsymbol{\rho}_\mathcal{K}$ is realized by $f_\mathcal{K} \geq 0$. However, the condition of strict realizability (12) is more restrictive than the natural condition $\rho_\mathcal{K}, T_\mathcal{K} > 0$ (see [26] for a counter example). But, as it is stated in the following theorem, it is sufficient to have an initial condition $f^0_\mathcal{K}$ strictly positive to ensure that $\boldsymbol{\rho}_\mathcal{K}$ is always strictly realizable.*

THEOREM 3.2. *Let $f^0_\mathcal{K}$ be a strictly positive vector of $\mathbf{R}^{N_v}$. Consider the initial value problem associated with model (10), where $\mathcal{E}_\mathcal{K}[\boldsymbol{\rho}_\mathcal{K}]$ is defined by $(\mathcal{P}_\mathcal{K})$. If this problem has a solution $f_\mathcal{K}$, then the solution $f_\mathcal{K}$ remains strictly positive and thus the discrete equilibrium has always the form $\mathcal{E}_\mathrm{k}[\boldsymbol{\rho}_\mathcal{K}] = \exp(\boldsymbol{\alpha} \cdot \boldsymbol{m}(v_\mathrm{k}))$. Moreover, the model satisfies the conservation laws and the dissipation of entropy*

$$\partial_t \langle \boldsymbol{m} f_\mathcal{K} \rangle_\mathcal{K} + \nabla_\mathrm{x} \langle \boldsymbol{m} v f_\mathcal{K} \rangle_\mathcal{K} = 0, \quad \partial_t \langle f_\mathcal{K} \log f_\mathcal{K} \rangle_\mathcal{K} + \nabla_\mathrm{x} \langle v f_\mathcal{K} \log f_\mathcal{K} \rangle_\mathcal{K} \leq 0.$$

Note here that these properties permit us to obtain existence and uniqueness results for model (10), as well as convergence toward the continuous BGK (see [25]).

Velocity discretization of the BGK-ES model.

Following the previous approach, we define the approximation $\mathcal{G}_\mathcal{K}[f_\mathcal{K}]$ of $G[f]$ by a discrete version of the generalized entropy minimization problem (8). Then we have

$$\mathcal{G}_\mathrm{k}[f_\mathcal{K}] = \exp(\vec{\alpha} \cdot \vec{m}(v_\mathrm{k})),$$

where $\vec{m}(v_\mathrm{k}) = (1, v_\mathrm{k}, v_\mathrm{k} \otimes v_\mathrm{k})^T$ and $\vec{\alpha}$ is the unique solution of the following non-linear system of ten equations (six only for plane flows)

$$\langle \vec{m} \exp(\vec{\alpha} \cdot \vec{m}) \rangle_\mathcal{K} = (\rho_\mathcal{K}, \rho_\mathcal{K} u_\mathcal{K}, \rho_\mathcal{K} u_\mathcal{K} \otimes u_\mathcal{K} + \rho \mathcal{T}_\mathcal{K}).$$

However, note that the modified tensor $\mathcal{T}_\mathcal{K}$ should now be defined as

$$\mathcal{T}_\mathcal{K} = \frac{1}{Pr} \Pi_\mathcal{K} + (1 - \frac{1}{Pr}) \Theta_\mathcal{K},$$

where $\rho_\mathcal{K} \Pi_\mathcal{K} = \langle (v - u_\mathcal{K}) \otimes (v - u_\mathcal{K}) \mathcal{E}_\mathcal{K}[\boldsymbol{\rho}_\mathcal{K}] \rangle_\mathcal{K}$ is the stress tensor of the discrete equilibrium $\mathcal{E}_\mathcal{K}[\boldsymbol{\rho}_\mathcal{K}]$. As opposed to the continuous case, $\rho_\mathcal{K} \Pi_\mathcal{K}$ is different from $\rho_\mathcal{K} R T_\mathcal{K} I$, because of a lack of symmetry and invariance of the discrete velocity set. This modification is necessary to ensure the equilibrium property, *i.e.* that the discrete collision operator is zero if and only if $f_\mathcal{K} = \mathcal{E}_\mathcal{K}[\boldsymbol{\rho}_\mathcal{K}]$. The discrete-velocity BGK-ES model is thus positive and conservative, but the entropy property seems more difficult to be rigorously obtained. Actually, the fact that the entropy of $G[f]$ is lower than the entropy of f relies for the continuous case on analytic expressions that are not available in the discrete case (see [2]). But as it will be shown in the next sections, computations using this model are possible and give accurate results.

Discretization of the diffuse reflection.

Using our approach, this boundary condition can be very naturally discretized. The wall Maxwellian $M[\boldsymbol{\rho}_w]$ of (9) is approximated by the discrete equilibrium $\mathcal{E}_{\mathrm{k}}[\boldsymbol{\rho}_w]$ associated to $\boldsymbol{\rho}_w$. We set

$$f_{\mathrm{k}}(t,\mathrm{x}) = \phi(\mathrm{x})\,\mathcal{E}_{\mathrm{k}}[\boldsymbol{\rho}_w], \quad v_{\mathrm{k}}\cdot n(\mathrm{x}) > 0. \tag{13}$$

The parameter $\phi(\mathrm{x})$ must be determined so as to avoid a mass flux across the wall. In the discrete frame, this yields

$$\phi(\mathrm{x}) = -\frac{\sum_{v_{\mathrm{k}}\cdot n(\mathrm{x})<0} v_{\mathrm{k}}\cdot n(\mathrm{x})\, f_{\mathrm{k}}(t,\mathrm{x})\Delta v_x\Delta v_y\Delta v_z}{\sum_{v_{\mathrm{k}}\cdot n(\mathrm{x})>0} v_{\mathrm{k}}\cdot n(\mathrm{x})\, \mathcal{E}_{\mathrm{k}}[\boldsymbol{\rho}_w]\Delta v_x\Delta v_y\Delta v_z} \tag{14}$$

4. CONSERVATIVE AND ENTROPIC DISCRETIZATION OF THE TRANSPORT OPERATOR: AXISYMMETRIC CASE

In this section, we consider a general kinetic equation

$$\partial_t f + v\cdot\nabla_{\mathrm{x}} f = C(f) \tag{15}$$

that could be BGK or BGK-ES, as well as Boltzmann or Fokker-Planck equation. First we make some remarks about cylindrical coordinates transformation of (15) in view of the discretization, and about conservation laws and dissipation of entropy. Then we give algebraic relations that should be satisfied by any finite difference discretization of the transport operator, independently of the discrete collision operator. We review some existing discretizations and our new schemes are presented. At last, an application to the BGK equation is given.

4.1. Conservation laws and entropy dissipation

The axisymmetric formulation of equation (15) is obtained as follows. Space variables are written in a system of cylindrical coordinates $(x,y,z) = (x, r\cos\varphi, r\sin\varphi)$, and in order to use the axial symmetry in space, we define the radial and azimuthal velocities v_r and v_φ by

$$v_r = v_y\cos\varphi + v_z\sin\varphi, \qquad v_\varphi = -v_y\sin\varphi + v_z\cos\varphi.$$

The assumption of axial symmetry now reads $\partial_\varphi f(t,x,r,\varphi,v_x,v_r,v_\varphi) = 0$, and the Cartesian equation (15) yields

$$\partial_t f + v_x\,\partial_x f + v_r\,\partial_r f + \frac{v_\varphi^2}{r}\,\partial_{v_r} f - \frac{v_r v_\varphi}{r}\,\partial_{v_\varphi} f = C(f). \tag{16}$$

Note the velocity gradients of f in this equation, that are in fact inertia terms due to the local coordinate system.

We feel it necessary to explain why this formulation is not convenient for a velocity discretization. The characteristic curves of transport equation (16) are more complex than for the Cartesian equation, because they are now curves of $\mathbf{R}^4$ defined by

$$\dot{x}(t) = v_x, \qquad \dot{r}(t) = v_r, \qquad \dot{v_r}(t) = \frac{v_\varphi^2}{r}, \qquad \dot{v_\varphi}(t) = -\frac{v_r v_\varphi}{r}.$$

However it can easily be seen that they satisfy $v_r(t)^2 + v_\varphi(t)^2 = cst$, which means that in the plane (v_r, v_φ), the characteristic curves are circles. Consequently, one can observe that in view of the discretization of (16), the bounded domain that would replace the velocity space should have a circular section in the plane (v_r, v_φ). Otherwise, due to the intersection of the characteristic curves with the boundary of the domain, boundary conditions in velocity would be needed. Therefore, it appears that, for a future discretization, a circular coordinate system for the radial and azimuthal velocities is more relevant than the previous rectangular system. As Sugimoto and Sone in [35], we define ζ and ω by $(v_r, v_\varphi) = (\zeta\cos\omega, \zeta\sin\omega)$, and equation (16) now reads as a much more convenient equation

$$\partial_t f + v_x\,\partial_x f + \zeta\cos\omega\,\partial_r f - \frac{\zeta\sin\omega}{r}\,\partial_\omega f = C(f). \tag{17}$$

A completely conservative form equation can be obtained

$$\partial_t rf + v_x\,\partial_x rf + \zeta\cos\omega\,\partial_r rf - \zeta\,\partial_\omega(\sin\omega f) = rC(f). \tag{18}$$

Now, we define the four moments density, axial and radial momentums, and total energy by

$$(\rho, \rho u_x, \rho u_r, E)^T = \int (1, v_x, \zeta\cos\omega, \tfrac{1}{2}(v_x^2+\zeta^2))^T f\,\zeta dv_x d\zeta d\omega. \tag{19}$$

The components of the stress tensor and of the heat flux are denoted by $\rho\Theta_{xx}$, $\rho\Theta_{rr}$, $\rho\Theta_{xr}$, $\rho\Theta_{\varphi\varphi}$ and q_x, q_r. For sake of simplicity, we have assumed that f is even in ω (*i.e.* $f(\omega) = f(-\omega)$), thus the tangential quantities $u_\varphi, \Theta_{r\varphi}, \Theta_{x\varphi}, q_\varphi$ are zero. This assumption, which is equivalent to $f(v_r, v_\varphi) = f(v_r, -v_\varphi)$, is valid for flows without incidence past axisymmetric bodies. The conservation laws and the dissipation of entropy are obtained by integrating (18) multiplied by $(1, v_x, \zeta\cos\omega, \frac{1}{2}(v_x^2+\zeta^2), 1+\log f)$. This yields

$$\partial_t r\rho + \partial_x r\rho u_x + \partial_r r\rho u_r = 0, \tag{20a}$$

$$\partial_t r\rho u_x + \partial_x r(\rho u_x^2 + \rho\Theta_{xx}) + \partial_r r(\rho u_x u_r + \rho\Theta_{xr}) = 0, \tag{20b}$$

$$\partial_t r\rho u_r + \partial_x r(\rho u_x u_r + \rho\Theta_{xr}) + \partial_r r(\rho u_r^2 + \rho\Theta_{rr}) = \rho\Theta_{\varphi\varphi}, \tag{20c}$$

$$\begin{aligned}\partial_t rE + \partial_x r(u_x E + \rho(\Theta_{xx}u_x + \Theta_{xr}u_r) + q_x)\\ + \partial_r r(u_r E + \rho(\Theta_{xr}u_x + \Theta_{rr}u_r) + q_r) = 0,\end{aligned} \tag{20d}$$

$$\begin{aligned}\partial_t r\int f\log f\,\zeta dv_x d\zeta d\omega + \partial_x r\int v_x f\log f\,\zeta dv_x d\zeta d\omega\\ + \partial_r r\int \zeta\cos\omega f\log f\,\zeta dv_x d\zeta d\omega \le 0.\end{aligned} \tag{20e}$$

In view of the velocity discretization of (18), we now discuss the intermediate steps between (18) and (20a-e). For instance, for the density, integrating (18) first yields

$$\partial_t r\rho + \partial_x r\rho u_x + \partial_r r\rho u_r = \int \zeta\,\partial_\omega(\sin\omega f)\,\zeta dv_x d\zeta d\omega + r\int C(f)\,\zeta dv_x d\zeta d\omega.$$

But the contribution of $C(f)$ is zero, as well as the contribution of ∂_ω, since we have

$$\int_0^{2\pi} \partial_\omega(\sin\omega f)\, d\omega = 0. \tag{21a}$$

Therefore we find (20a). For ρu_x and E, equations (20b) and (20d) are obtained for the same reasons. For ρu_r, Eq. (20c) is due to the following contribution of ∂_ω

$$\int_0^{2\pi} \cos\omega\, \partial_\omega(\sin\omega f)\, d\omega = \int_0^{2\pi} \sin^2\omega f\, d\omega. \tag{21b}$$

For the entropy, note that by assumption, the contribution of $C(f)$ is negative. Moreover, the contribution of ∂_ω is found to satisfy

$$\int_0^{2\pi} \partial_\omega(\sin\omega f)\log f\, d\omega \le \int_0^{2\pi} \cos\omega f\, d\omega. \tag{21c}$$

In fact, this relation is an equality, but the inequality is sufficient to obtain (20e). Finally, note that the uniform flows in t, x, r, ω are solution of (18). This is due to the trivial relation

$$\partial_\omega(\sin\omega) = \cos\omega. \tag{21d}$$

Consequently, it appears that analyzing the possible discretizations of the terms due to ∂_ω in the transport operator is essential to a conservative and entropic discrete-velocity model. In fact, this short study suggests that it is sufficient to satisfy some discrete relations similar to (21a-d). Obviously, this problem does not appear in Cartesian coordinates. Also note that this problem is different from the approximation of the source term, which has been treated in the previous section.

The same procedure can be adapted to the non-conservative form equation (17), and we obtain the same conservation laws and entropy dissipation. The different contributions of ∂_ω now read

$$\int_0^{2\pi} \sin\omega\, \partial_\omega f\, d\omega = -\int_0^{2\pi} \cos\omega f\, d\omega, \tag{22a}$$

$$\int_0^{2\pi} \cos\omega\sin\omega\, \partial_\omega f\, d\omega = \int_0^{2\pi} (-\cos^2\omega + \sin^2\omega) f\, d\omega, \tag{22b}$$

$$\int_0^{2\pi} \sin\omega\, \partial_\omega f(1+\log f)\, d\omega \le -\int_0^{2\pi} \cos\omega f\log f\, d\omega, \tag{22c}$$

$$\partial_\omega 1 = 0. \tag{22d}$$

The first relation appears for conservation of $\rho, \rho u_x, E$, the second one for ρu_r, the third one for the entropy, and the last relation is for uniform flows.

Finally, note that if f is not even in ω, then there exists an additional conservation law for ρu_φ with a source term. Relations similar to (21b) and (22b) can be derived.

4.2. Discretization of the velocity derivative

In this section, the discrete collision operator $C_{\mathcal{K}}(f)$ is assumed to be conservative and entropic (see section 3 for BGK and BGK-ES operators, see also [30] for Boltzmann, and [16] for Fokker-Planck). Then equation (15) with only the transport term is considered. The variable $\omega \in [0, 2\pi]$ is discretized by the points $\{\omega_q\}_{q=0}^{Q}$, and $f(\omega_q)$ is approximated by f_q. Since the problem of conservation and entropy is only due to the discretization of ω (see section 4.1), v_x and ζ are kept continuous.

Let D be a finite difference operator that approximates ∂_ω at least up to the first order. In the case of the conservative form equation (18), the term $\partial_\omega(\sin\omega f)$ is approximated by $D(\sin\omega f)_q$. Then the discrete approximation of (18) without collision term is

$$\partial_t r f_q + v_x\, \partial_x r f_q + \zeta \cos\omega_q\, \partial_r r f_q - \zeta D(\sin\omega f)_q = 0. \tag{23}$$

The macroscopic quantities are defined as in (19), except that integrals on $[0, 2\pi]$ are replaced by a simple rectangular formula. For instance, we set

$$(\rho, \rho u_x, \rho u_r, E)^T = \int_{\mathbf{R}} \int_0^{+\infty} \sum_{q\geq 0} (1, v_x, \zeta\cos\omega_q, \tfrac{1}{2}(v_x^2+\zeta^2))^T f_q(v_x,\zeta)\, \Delta\omega\, dv_x \zeta d\zeta. \tag{24}$$

Now the discrete approximations of relations (21a-d) read as algebraic relations for the operator D

$$\sum_q D(\sin\omega f)_q = 0, \tag{25a}$$

$$\sum_q \cos\omega_q D(\sin\omega f)_q = \sum_q \sin^2\omega_q f_q, \tag{25b}$$

$$\sum_q D(\sin\omega f)_q \log f_q \leq \sum_q \cos\omega_q f_q, \tag{25c}$$

$$D(\sin\omega)_q = \cos\omega_q. \tag{25d}$$

The advantage of these relations is that we can prove, exactly as for the continuous equation (18), that they are sufficient to obtain the conservation laws for the discrete moments as defined by (24), the dissipation of discrete entropy, and the preservation of uniform flows. This is stated in the following result:

PROPOSITION 4.1. *Let $f = \{f_q\}_{q=0}^{Q}$ be a solution of (23), then*

- *the discrete moments $\rho, \rho u_x, E$ satisfy the conservation laws (20a,20b,20d)) if (25a) is satisfied;*
- *the discrete radial momentum ρu_r satisfies the conservation law with source term (20c) if (25b) holds;*
- *the discrete entropy $\int_{\mathbf{R}} \int_0^{+\infty} \sum_{q\geq 0} f_q \log f_q\, \Delta\omega\, dv_x \zeta d\zeta$ satisfies dissipation relation (20e) if (25c) holds;*
- *uniform flows (in t, x, r, q) are preserved if (25d) is satisfied.*

For the non-conservative form equation (17), the term $\partial_\omega f$ is approximated by $D(f)_q$. The discrete approximation of (17) without collision term is

$$\partial_t f_q + v_x\,\partial_x f_q + \zeta\cos\omega_q\,\partial_r f_q - \frac{\zeta\sin\omega_q}{r} D(f)_q = 0. \tag{26}$$

As for the conservative form equation, the following discrete formulations of relations (22a-d) are sufficient to obtain the conservation laws and entropy dissipation, and to preserve uniform flows

$$\sum_q \sin\omega_q D(f)_q = -\sum_q \cos\omega_q f_q, \tag{27a}$$

$$\sum_q \cos\omega_q \sin\omega_q D(f)_q = \sum_q (-\cos^2\omega_q + \sin^2\omega_q) f_q, \tag{27b}$$

$$\sum_q \sin\omega_q D(f)_q (1+\log f_q) \le -\sum_q \cos\omega_q f_q \log f_q, \tag{27c}$$

$$D(1)_q = 0. \tag{27d}$$

Note that the operator D should preserve the positivity of f, but as opposed to conservation properties, this is not expressed by an algebraic relation for D.

REMARK 4.3. *Since the radial momentum ρu_r is not a conserved quantity by its own (there is a source term in (20c)), it is important to address the issue concerning the conservation of the total momentum $\int(\rho u)\,r dx dr d\varphi$, where u is the vector $u = u_x e_x + u_r e_r$ in the cylindrical basis (e_x, e_r, e_φ). The assumption of axial symmetry $\partial_\varphi = 0$ implies that the sum of the contributions of the radial momentum is zero. Hence the total momentum is parallel to the axis, i.e.*

$$\int(\rho u)\,r dx dr d\varphi = \left(\int(\rho u_x)\,r dx dr d\varphi\right) e_x.$$

Consequently, this total momentum is conserved, provided that the local conservation law of ρu_x is satisfied. From proposition 4.1, a sufficient condition is that (25a) or (27a) holds.

4.3. Two operators used in literature

The following upwind operators are defined for the non-conservative form equation (26). They are presented here with the assumption that f is even in ω, and therefore for $\omega_q \in [0, \pi]$ only.

The first one is defined by a first order upwind discretization, used by Shakhov in [31].

$$D(f)_q = \frac{f_{q+1} - f_q}{\Delta\omega}. \tag{28}$$

In the sequel, the discrete equation (26) with this operator will be denoted by UNCE. It can be seen that this method preserves the positivity of f and uniform flows, since (25d) is satisfied.

The second operator is defined by a second order upwind discretization, used by Sone et al. in [35]

$$D(f)_q = \frac{1}{\Delta\omega}(-\frac{1}{2}f_{q+2} + 2f_{q+1} - \frac{3}{2}f_q). \tag{29}$$

This will be denoted by U2NCE. This operator preserves uniform flows, but not the positivity of f.

Whereas this discretization is second order accurate, note that the conservation laws are obtained at order $O(\Delta\omega)$ only, as for the operator UNCE. Moreover, for these two methods, the entropy is not dissipated.

4.4. Trigonometric corrections

The fact that the two previous methods do not satisfy the conservation laws can be explained as follows. When one tries to prove that relation (27a) holds, one makes discrete integration by parts, and there appears the adjoint operator D^* of D, defined by

$$\sum_q D(f)_q g_q = \sum_q f_q D^*(g)_q + \text{boundary terms}, \tag{30}$$

for any functions f, g. Then, relation (27a) is obtained if the boundary terms vanish and if D^* is *exact* for the sine function. Our idea is then to modify the previous operators so as to make the adjoint D^* exact for the trigonometric functions.

For UNCE, we replace D of (28) by

$$D(f)_q = \frac{f_{q+1} - \cos\Delta\omega f_q}{\sin\Delta\omega}.$$

This operator, denoted by T-UNCE, is an asymptotically equivalent approximation to (28) as $\Delta\omega$ goes to zero, thus it is consistent. It can easily be proved that D and D^* are exact for sine and cosine. Then discrete equation (26) has the following properties : positivity of f, conservation of ρ, ρu_x, E. However, since $D^*(\cos\omega\sin\omega)_q = -\cos^2\omega_q + \sin^2\omega_q + O(\Delta\omega)$, then we do not have conservation law for ρu_r. Moreover, we have $D(1)_q = \frac{1-\cos\Delta\omega}{\sin\Delta\omega} = 1 + O(\Delta\omega)$, thus this scheme does not preserve uniform flows. This last property is known to lead to schemes that are not precise and not robust.

For U2NCE, we replace D of (29) by

$$D(f)_q = \frac{1}{\sin\Delta\omega}\Big(-\frac{1}{2}f_{q+2} + (1+\cos\Delta\omega)f_{q+1} - \frac{1+2\cos\Delta\omega}{2}f_q\Big).$$

This operator, denoted by T-U2NCE is also a consistent approximation of ∂_ω. It is exact for sine and cosine, and preserves uniform flows. But due to the non-vanishing boundary terms, this is not sufficient to ensure conservation. Namely, the conservation laws are satisfied only up to the first order.

4.5. New trigonometric operators for the conservative form equation

We propose the following operator

$$D(\sin\omega f)_q = \frac{\sin\omega_{q+1}f_{q+1} - \sin\omega_{q-1}f_{q-1}}{2\sin\Delta\omega}. \tag{31}$$

This is nothing but a classical centered finite difference approximation of second order, where we have replaced the increment $\Delta\omega$ by the asymptotically equivalent quantity $\sin\Delta\omega$. Thus this formula is consistent. The corresponding discrete equation (23) will be denoted by T-CCE. In order to eliminate the boundary terms in (30), we set $\omega_0 = 0$ and $\omega_Q = 2\pi - \Delta\omega$. Then (25a) is satisfied, which implies (thanks to proposition 4.1) that we have the conservation laws for $\rho, \rho u_x, E$. For ρu_r and uniform flows, note that owing to our trigonometric correction ($\Delta\omega \to \sin\Delta\omega$), then D and $D^* = -D$ satisfy

$$D(\cos\omega)_q = -\sin\omega_q, \qquad D(\sin\omega)_q = \cos\omega_q,$$

Thus (25b) and (25d) are satisfied, and we have the conservation law of ρu_r and the uniform flows are preserved. However, this centered operator does not preserve the positivity of f, so we can not prove the entropy property. We also mention that the operator without the trigonometric correction ($D(f)_q = \frac{f_{q+1}-f_{q-1}}{2\Delta\omega}$) only satisfies the conservation laws of $\rho, \rho u_x, E$. It will be denoted by CCE.

REMARK 4.4. *Note that we can use the centered operator $D(f)_q = \frac{f_{q+1}-f_{q-1}}{2\Delta\omega}$ for the non-conservative form equation (26), it will be denoted by CNCE. The only property of this scheme is the preservation of uniform flows. As for the conservative form equation, we can derive the following trigonometric modification $D(f)_q = \frac{f_{q+1}-f_{q-1}}{2\sin\Delta\omega}$. Then we obtain the additional property of conservation of ρ, ρu_x, and E. This scheme will be denoted by T-CNCE.*

Finally, we propose an upwind version of the previous operator defined in (31) so as to obtain the positivity. We set

$$\begin{aligned} D(\sin\omega f)_q \;=\; & \frac{1}{2\sin\frac{\Delta\omega}{2}}\Big(((\sin\omega_{q+\frac12})^+ f_{q+1} + (\sin\omega_{q+\frac12})^- f_q) \\ & -((\sin\omega_{q-\frac12})^+ f_q + (\sin\omega_{q-\frac12})^- f_{q-1})\Big), \end{aligned} \tag{32}$$

where $a^\pm$ denotes $\frac12(a \pm |a|)$ and $\omega_{q\pm\frac12} = \omega_q \pm \frac{\Delta\omega}{2}$. Since $2\sin\frac{\Delta\omega}{2}$ and $\Delta\omega$ are asymptotically equivalent, this formula is consistent. The boundary terms in discrete integrations by parts are eliminated by setting $Q = 2m-1$ with m such that $\omega_m = \pi$. The discrete equation (23) with this operator will be denoted by T-UCE. This equation possesses numerous properties that are stated in the following result:

PROPOSITION 4.2.

(i)the positivity of f is preserved;
(ii)the conservation laws of $\rho, \rho u_x, E$ are satisfied (Eq. (20a,20b,20d));
(iii)the entropy is locally dissipated (Eq. (20e)).
(iv)the uniform flows are preserved;

Proof. Property (iv) is obtained by noting that (25d) is satisfied

$$D(\sin\omega)_q = \frac{1}{2\sin\frac{\Delta\omega}{2}}(\sin\omega_{q+\frac12} - \sin\omega_{q-\frac12}) = \cos\omega_q.$$

For (ii), we note that $D(\sin\omega f)_q$ can be written as a numerical flux difference $D(\sin\omega f)_q = h_{q+\frac{1}{2}} - h_{q-\frac{1}{2}}$, therefore (25a) is obvious. Property (i) is due to the upwinding of the discretization.

The most striking property of this discretization is the entropy dissipation. It can actually be proved that (25c) holds: by a change of indexes, it comes

$$\sum_{q=0}^{Q} D(\sin\omega f)_q \log f_q \;=\; \sum_{q=0}^{Q} \frac{1}{2\sin\frac{\Delta\omega}{2}}\Big((\sin\omega_{q-\frac{1}{2}})^+ \log f_{q-1} + (\sin\omega_{q+\frac{1}{2}})^- \log f_q \\ -(\sin\omega_{q-\frac{1}{2}})^+ \log f_q - (\sin\omega_{q+\frac{1}{2}})^- \log f_{q+1}\Big) f_q.$$

Then we use the convexity inequality $t_2 \log t_1 \le t_2 \log t_2 + t_1 - t_2$ for the terms $f_q \log f_{q\pm1}$; the logarithms vanish and we obtain

$$\sum_{q=0}^{Q} D(\sin\omega f)_q \log f_q \;\le\; \sum_{q=0}^{Q} \frac{1}{2\sin\frac{\Delta\omega}{2}}\Big((\sin\omega_{q-\frac{1}{2}})^+ (f_{q-1} - f_q) \\ -(\sin\omega_{q+\frac{1}{2}})^- (f_{q+1} - f_q)\Big).$$

By a new change of indexes, we find

$$\begin{aligned} &\sum_{q=0}^{Q} D(\sin\omega f)_q \log f_q \\ \le\; &\sum_{q=0}^{Q} \frac{1}{2\sin\frac{\Delta\omega}{2}}\Big((\sin\omega_{q+\frac{1}{2}})^+ - (\sin\omega_{q-\frac{1}{2}})^+ - (\sin\omega_{q-\frac{1}{2}})^- + (\sin\omega_{q+\frac{1}{2}})^-\Big) f_q \\ =\; &\sum_{q=0}^{Q} \cos\omega_q f_q. \end{aligned}$$

This is (25c), which implies (iii) (cf. proposition 4.1). ■

REMARK 4.5. *To our knowledge, it is the first time that a discretization preserving the positivity, the conservation of ρ, ρu_x et E, and the entropy dissipation, is presented. Also note that if the classical upwind discretization is used without trigonometric correction (i.e. with $\Delta\omega$ instead of $2\sin\frac{\Delta\omega}{2}$ in (32), that will be denoted by UCE), then we have only $D(\sin\omega)_q = \cos\omega_q + O(\Delta\omega)$, and only properties (ii) and (i) are satisfied.*

REMARK 4.6. *The evolution equation of ρu_r (20c) is obtained at order $O(\Delta\omega)$ only. But we think it less important to be obtained than the other properties. In fact, equation (20c) possesses a source term, therefore even in continuous case, the quantity ρu_r is not really conserved.*

4.6. Summary of the different discretizations and their related properties

For the readability of the sequel, we summarize in this section all the previous schemes. The discretizations of the velocity derivative for the conservative form equation (18) are the following

$$\begin{aligned}
\text{CCE} : D(\sin\omega f)_q &= \frac{\sin\omega_{q+1} f_{q+1} - \sin\omega_{q-1} f_{q-1}}{2\Delta\omega},\\
\text{T}-\text{CCE} : D(\sin\omega f)_q &= \frac{\sin\omega_{q+1} f_{q+1} - \sin\omega_{q-1} f_{q-1}}{2\sin\Delta\omega},\\
\text{UCE} : D(\sin\omega f)_q &= \frac{1}{\Delta\omega}\Big(((\sin\omega_{q+\frac12})^+ f_{q+1} + (\sin\omega_{q+\frac12})^- f_q)\\
&\qquad -((\sin\omega_{q-\frac12})^+ f_q + (\sin\omega_{q-\frac12})^- f_{q-1})\Big),\\
\text{T}-\text{UCE} : D(\sin\omega f)_q &= \frac{1}{2\sin\frac{\Delta\omega}{2}}\Big(((\sin\omega_{q+\frac12})^+ f_{q+1} + (\sin\omega_{q+\frac12})^- f_q)\\
&\qquad -((\sin\omega_{q-\frac12})^+ f_q + (\sin\omega_{q-\frac12})^- f_{q-1})\Big).
\end{aligned}$$

For the non-conservative form equation (17), we have

$$\begin{aligned}
\text{CNCE} : D(f)_q &= \frac{f_{q+1} - f_{q-1}}{2\Delta\omega},\\
\text{T}-\text{CNCE} : D(f)_q &= \frac{f_{q+1} - f_{q-1}}{2\sin\Delta\omega},\\
\text{UNCE} : D(f)_q &= \frac{f_{q+1} - f_q}{\Delta\omega},\\
\text{T}-\text{UNCE} : D(f)_q &= \frac{f_{q+1} - \cos\Delta\omega f_q}{\sin\Delta\omega},\\
\text{U2NCE} : D(f)_q &= \frac{1}{\Delta\omega}(-\frac12 f_{q+2} + 2f_{q+1} - \frac32 f_q),\\
\text{T}-\text{U2NCE} : D(f)_q &= \frac{1}{\sin\Delta\omega}\Big(-\frac12 f_{q+2} + (1+\cos\Delta\omega) f_{q+1} - \frac{1+2\cos\Delta\omega}{2} f_q\Big).
\end{aligned}$$

We recall that the schemes CCE, T-CCE, UCE and T-UCE are the new schemes that have been proposed in section 4.5 for the conservative form equation, as well as CNCE and T-CNCE for the non-conservative form equation. Schemes UNCE and U2NCE have been respectively proposed in [31] and [35]. They are recalled in section 4.3 of the present paper. Finally, their trigonometric corrections T-UNCE and T-U2NCE have been proposed in section 4.4. The properties of all these schemes are recalled in table 1.

Note that another approach has recently been proposed by Larina and Rykov [22]. By a modification of the radial velocity $\zeta\cos\omega$, they obtain a second order conservative scheme (for $\rho, \rho u_x, \rho u_r, E$), but non positive. If we replace $\Delta\omega$ by $\sin\Delta\omega$ in their method, it reduces to our scheme T-CCE.

4.7. Application to the BGK equation

In order to apply the previous discretizations to the BGK equation, we discretize the velocity variables v_x and ζ by

$$v_x^k = k\Delta v_x + a, \qquad \zeta_l = l\Delta\zeta,$$

with $\mathrm{k} = (k, l, q) \in \mathcal{K}$ (cf. section 3). The fully discrete-velocity models for the non-conservative and conservative axisymmetric kinetic equations are

$$\partial_t f_\mathrm{k} + v_x^k \, \partial_x f_\mathrm{k} + \zeta_l \cos\omega_q \, \partial_r f_\mathrm{k} - \frac{\zeta_l \sin\omega_q}{r} D(f_{k,l})_q = C(f_\mathcal{K})_\mathrm{k}, \tag{33}$$

$$\partial_t r f_\mathrm{k} + v_x^k \, \partial_x r f_\mathrm{k} + \zeta_l \cos\omega_q \, \partial_r r f_\mathrm{k} - \zeta_l D(\sin\omega f_{k,l})_q = r C(f_\mathcal{K})_\mathrm{k}, \tag{34}$$

where $f_{k,l} = (f_{k,l,q})_{q=0\ldots Q}$. In the case of the BGK equation, the discrete collision operator is

$$C(f_\mathcal{K})_\mathrm{k} = \frac{1}{\tau}(\mathcal{E}_\mathrm{k}[\boldsymbol{\rho}_\mathcal{K}] - f_\mathrm{k}).$$

According to section 3, $\mathcal{E}_\mathrm{k}[\boldsymbol{\rho}_\mathcal{K}]$ is the discrete equilibrium defined by $\mathcal{E}_\mathrm{k}[\boldsymbol{\rho}_\mathcal{K}] = \exp(\boldsymbol{\alpha} \cdot \boldsymbol{m}(v_\mathrm{k}))$, where $\boldsymbol{m}(v_\mathrm{k}) = (1, v_x^k, \zeta_l \cos\omega_q, \zeta_l \sin\omega_q, \frac{1}{2}(|v_x^k|^2 + \zeta_l^2))^T$, and the vector $\boldsymbol{\alpha}$ is the unique solution of the nonlinear system of five equations

$$\sum_\mathrm{k} \boldsymbol{m}(v_\mathrm{k}) \exp(\boldsymbol{\alpha} \cdot \boldsymbol{m}(v_\mathrm{k})) \, \zeta_l \Delta v_x \Delta\zeta \Delta\omega = (\rho, \rho u_x, \rho u_r, \rho u_\varphi, E).$$

Note that if the distribution function is even in ω, then $u_\varphi = 0$, and the system above reduces to four equations only. This is also true if $u_x = 0$.

TABLE 1
Properties of the discrete-velocity models for the axisymmetric transport operator.

	uniform flows	positivity	cons. $\rho, \rho u_x, E$	cons. ρu_r	entropy
CCE	**yes**	*no*	*no*	*no*	*no*
T-CCE	**yes**	*no*	**yes**	**yes**	*no*
UCE	*no*	**yes**	**yes**	*no*	*no*
T-UCE	**yes**	**yes**	**yes**	*no*	**yes**
CNCE	**yes**	*no*	*no*	*no*	*no*
T-CNCE	**yes**	*no*	**yes**	*no*	*no*
UNCE	**yes**	**yes**	*no*	*no*	*no*
T-UNCE	*no*	**yes**	**yes**	*no*	*no*
U2NCE	**yes**	*no*	*no*	*no*	*no*
T-U2NCE	**yes**	*no*	*no*	*no*	*no*

5. DISCRETIZATION IN SPACE AND TIME OF THE DISCRETE-VELOCITY MODELS

In this section, we give an explicit scheme and a linearized implicit scheme for fast computing steady flows. The linear solver for solving the large linear systems is detailed. The algorithm for computing the discrete equilibrium is also given. The extension of these schemes to axisymmetric models is discussed at the end of the section.

5.1. Explicit scheme

For the sake of simplicity, our scheme is presented here in two spatial dimensions on a Cartesian grid, but all the properties stated here are valid for a 3-dimensional space and curvilinear meshes (cf. below). The equation to be approximated is

$$\partial_t f_{\rm k} + v_x^k \partial_x f_{\rm k} + v_y^l \partial_y f_{\rm k} = \frac{1}{\tau}(\mathcal{E}_{\rm k}[\boldsymbol{\rho}_{\mathcal{K}}] - f_{\rm k}), \qquad {\rm k} \in \mathcal{K}. \tag{35}$$

Note that in the case of plane flows, the dependency of $f_{\mathcal{K}}$ on v_z can be eliminated by introducing reduced distribution functions (see [36]). But this technique is not used here because it is not possible for axisymmetric flows, and we want a same scheme for both 2D plane and axisymmetric flows. Consider a spatial Cartesian grid defined by nodes $(x_i, y_j) = (i\Delta x, j\Delta y)$ and cells $]x_{i-\frac{1}{2}}, x_{i+\frac{1}{2}}[\times]y_{j-\frac{1}{2}}, y_{j+\frac{1}{2}}[$. Consider also a time discretization with $t_n = n\Delta t$. If $f_{i,j}^n = (f_{{\rm k},i,j}^n)_{{\rm k}\in\mathcal{K}}$ is an approximation of $f_{\mathcal{K}}(t_n, x_i, y_j)$, the moments of $f_{i,j}^n$ are naturally $\boldsymbol{\rho}_{i,j}^n = \langle \boldsymbol{m} f_{i,j}^n \rangle_{\mathcal{K}}$, and the corresponding discrete equilibrium is denoted by $(\mathcal{E}_{\rm k}[\boldsymbol{\rho}_{i,j}^n])_{{\rm k}\in\mathcal{K}}$. If $\boldsymbol{\rho}_{i,j}^n$ is strictly realizable (in the sense of (12)), the discrete equilibrium is therefore $\mathcal{E}_{\rm k}[\boldsymbol{\rho}_{i,j}^n] = \exp(\boldsymbol{\alpha}_{i,j}^n \cdot \boldsymbol{m}(v_{\rm k}))$, where $\boldsymbol{\alpha}_{i,j}^n$ is the unique solution of the system of four nonlinear equations (see remark 3.1)

$$\langle \boldsymbol{m} \exp(\boldsymbol{\alpha}_{i,j}^n \cdot \boldsymbol{m}) \rangle_{\mathcal{K}} = \boldsymbol{\rho}_{i,j}^n. \tag{36}$$

The transport part is simply the linear convection equation, and can be approximated by a standard finite volume scheme. For the nonlinear relaxation term, a standard centered approximation technique is used. Our scheme thus reads

$$\begin{aligned} f_{{\rm k},i,j}^{n+1} = f_{{\rm k},i,j}^n \;&-\; \frac{\Delta t}{\Delta x}(\mathcal{F}_{{\rm k},i+\frac{1}{2},j}^n - \mathcal{F}_{{\rm k},i-\frac{1}{2},j}^n) - \frac{\Delta t}{\Delta y}(\mathcal{F}_{{\rm k},i,j+\frac{1}{2}}^n - \mathcal{F}_{{\rm k},i,j-\frac{1}{2}}^n) \\ &+\; \frac{\Delta t}{\tau_{i,j}^n}(\mathcal{E}_{\rm k}[\boldsymbol{\rho}_{i,j}^n] - f_{{\rm k},i,j}^n), \end{aligned} \tag{37}$$

where the numerical fluxes are defined by

$$\begin{aligned} \mathcal{F}_{{\rm k},i+\frac{1}{2},j}^n &= \frac{1}{2}\left(v_x^k (f_{{\rm k},i+1,j}^n + f_{{\rm k},i,j}^n) - |v_x^k| (\Delta f_{{\rm k},i+\frac{1}{2},j}^n - \Phi_{{\rm k},i+\frac{1}{2},j}^n) \right) \\ \mathcal{F}_{{\rm k},i,j+\frac{1}{2}}^n &= \frac{1}{2}\left(v_y^l (f_{{\rm k},i,j+1}^n + f_{{\rm k},i,j}^n) - |v_y^l| (\Delta f_{{\rm k},i,j+\frac{1}{2}}^n - \Phi_{{\rm k},i,j+\frac{1}{2}}^n) \right) \end{aligned}$$

with the notation $\Delta f_{{\rm k},i+\frac{1}{2},j}^n = f_{{\rm k},i+1,j}^n - f_{{\rm k},i,j}^n$, and the flux limiter function $\Phi_{{\rm k},i+\frac{1}{2},j}^n$ allows to obtain a second order scheme. For instance $\Phi_{{\rm k},i+\frac{1}{2},j}^n = 0$ for first order, and $\Phi_{{\rm k},i+\frac{1}{2},j}^n = \text{minmod}(\Delta f_{{\rm k},i-\frac{1}{2},j}^n, \Delta f_{{\rm k},i+\frac{1}{2},j}^n, \Delta f_{{\rm k},i+\frac{3}{2},j}^n)$ for second order.

With the appropriate definitions of our discrete-velocity model, our scheme now possesses the expected properties. In the case of an infinite space domain (*i.e.* $(i,j) \in \mathbf{Z}^2$), theorem 3.2 can be expressed in its numerical form (proved in [26]):

PROPOSITION 5.1. *Let $\{f^0_{k,i,j}\}_{k,i,j}$ be a strictly positive initial condition. If the time steps follows the condition*

$$\Delta t \left(\max_{i,j}(\frac{1}{\tau^n_{i,j}}) + \max_{\mathcal{K}} \left(\frac{|v^k_x|}{\Delta x} + \frac{|v^l_y|}{\Delta y} \right) \right) < 1, \tag{38}$$

then the sequence $\{f^n\}_{n\geq 0}$ defined by the first order scheme (37) remains strictly positive, and the discrete equilibrium is $\mathcal{E}_{\mathrm{k}}[\boldsymbol{\rho}^n_{i,j}] = \exp(\boldsymbol{\alpha}^n_{i,j} \cdot \boldsymbol{m}(v_{\mathrm{k}}))$. Furthermore, the total mass, momentum, and energy are conserved, and the total entropy is decreasing.

General geometries are treated with a curvilinear mesh. Then we use the curvilinear coordinates $\xi(x,y)$ and $\eta(x,y)$ so as to approximate space derivatives on the grid. After this change of variables, equation (35) yields

$$\frac{1}{J}\partial_t f_{\mathrm{k}} + \partial_\xi\Big(v_{\mathrm{k}} \cdot \frac{\nabla\xi}{J} f_{\mathrm{k}}\Big) + \partial_\eta\Big(v_{\mathrm{k}} \cdot \frac{\nabla\eta}{J} f_{\mathrm{k}}\Big) = \frac{1}{J\tau}(\mathcal{E}_{\mathrm{k}}[\boldsymbol{\rho}_{\mathcal{K}}] - f_{\mathrm{k}}),$$

where $\nabla\xi = (\partial_x\xi, \partial_y\xi)$, $\nabla\eta = (\partial_x\eta, \partial_y\eta)$, and $J = \partial_x\xi\partial_y\eta - \partial_y\xi\partial_x\eta$. If we define a uniform grid ($\xi_i = i\Delta\xi, \eta_j = j\Delta\eta$), then a scheme very similar to (37) can be used

$$\begin{aligned} f^{n+1}_{\mathrm{k},i,j} = f^n_{\mathrm{k},i,j} \; &- \; \frac{\Delta t}{\Delta\xi}(\mathcal{F}^n_{\mathrm{k},i+\frac{1}{2},j} - \mathcal{F}^n_{\mathrm{k},i-\frac{1}{2},j})J_{i,j} - \frac{\Delta t}{\Delta\eta}(\mathcal{F}^n_{\mathrm{k},i,j+\frac{1}{2}} - \mathcal{F}^n_{\mathrm{k},i,j-\frac{1}{2}})J_{i,j} \\ &+ \; \frac{\Delta t}{\tau^n_{i,j}}(\mathcal{E}_{\mathrm{k}}[\boldsymbol{\rho}^n_{i,j}] - f^n_{\mathrm{k},i,j}), \end{aligned}$$

where the numerical fluxes are defined by

$$\begin{aligned} \mathcal{F}^n_{\mathrm{k},i+\frac{1}{2},j} \; &= \; \frac{1}{2}\left(v_{\mathrm{k}} \cdot \Big(\frac{\nabla\xi}{J}\Big)_{i+\frac{1}{2},j} (f^n_{\mathrm{k},i+1,j} + f^n_{\mathrm{k},i,j}) \right. \\ &\qquad \left. - \Big| v_{\mathrm{k}} \cdot (\frac{\nabla\xi}{J})_{i+\frac{1}{2},j} \Big| (\Delta f^n_{\mathrm{k},i+\frac{1}{2},j} - \Phi^n_{\mathrm{k},i+\frac{1}{2},j}) \right) \\ \mathcal{F}^n_{\mathrm{k},i,j+\frac{1}{2}} \; &= \; \frac{1}{2}\left(v_{\mathrm{k}} \cdot \Big(\frac{\nabla\eta}{J}\Big)_{i,j+\frac{1}{2}} (f^n_{\mathrm{k},i,j+1} + f^n_{\mathrm{k},i,j}) \right. \\ &\qquad \left. - \Big| v_{\mathrm{k}} \cdot (\frac{\nabla\eta}{J})_{i,j+\frac{1}{2}} \Big| (\Delta f^n_{\mathrm{k},i,j+\frac{1}{2}} - \Phi^n_{\mathrm{k},i,j+\frac{1}{2}}) \right). \end{aligned}$$

The geometric coefficients $(\frac{\nabla\xi}{J})_{i\pm\frac{1}{2},j}$, $(\frac{\nabla\eta}{J})_{i,j\pm\frac{1}{2}}$ and $J_{i,j}$ are standard approximations used in order to preserve the free stream. This scheme has the same properties as scheme (37) (*i.e.* positivity, conservation of moments, dissipation of entropy), provided that a CFL condition similar to (38) be satisfied.

REMARK 5.7. *The same scheme is used with the BGK-ES model by replacing $\mathcal{E}_{\mathrm{k}}[\boldsymbol{\rho}^n_{i,j}]$ by $\mathcal{G}_{\mathrm{k}}[f^n_{i,j}]$.*

5.2. Linearized implicit scheme for steady flows

In steady state computations, CFL condition (38) of the explicit scheme is very restrictive for dense or rapid regimes. A classical way to overcome this difficulty is to use an implicit scheme. It is derived from the explicit scheme by evaluating at t_{n+1} the terms that produce undesirable negative distributions for large Δt.

5.2.1. Description of the scheme

In the collision operator, the loss term $(-f^n_{\mathrm{k},i,j})$ is negative and then it is written at t_{n+1}. The gain term, namely the discrete equilibrium $\mathcal{E}_\mathrm{k}[\boldsymbol{\rho}^n_{i,j}]$, is positive, and therefore may be kept explicit (a strategy used in [36]). However, gain and loss terms are then evaluated at different times, which is observed to slow the convergence of the scheme considerably (see [26]). Consequently, we decide to evaluate the gain term at t_{n+1} as well. However, defining an implicit relaxation time $\tau^{n+1}_{i,j}$ is not very useful. Since the discrete equilibrium is a nonlinear function of f, it may be linearized as follows

$$\mathcal{E}_\mathrm{k}[\boldsymbol{\rho}^{n+1}_{i,j}] \approx \mathcal{E}_\mathrm{k}[\boldsymbol{\rho}^n_{i,j}] + [\mathcal{D}^n_{i,j}(f^{n+1}_{i,j} - f^n_{i,j})]_\mathrm{k},$$

where $\mathcal{D}^n_{i,j}$ is the Jacobian of the mapping $g \in \mathbf{R}^{N_v} \mapsto \mathcal{E}[g]$ evaluated at $f^n_{i,j}$. Then the *linearized implicit* first order scheme is the following

$$\begin{aligned} f^{n+1}_{\mathrm{k},i,j} \;+\; & \frac{\Delta t}{\Delta x}(\mathcal{F}^{n+1}_{\mathrm{k},i+\frac12,j} - \mathcal{F}^{n+1}_{\mathrm{k},i-\frac12,j}) + \frac{\Delta t}{\Delta y}(\mathcal{F}^{n+1}_{\mathrm{k},i,j+\frac12} - \mathcal{F}^{n+1}_{\mathrm{k},i,j-\frac12}) \\ + \; & \frac{\Delta t}{\tau^n_{i,j}}(f^{n+1}_{\mathrm{k},i,j} - [\mathcal{D}^n_{i,j} f^{n+1}_{i,j}]_\mathrm{k}) = f^n_{\mathrm{k},i,j} + \frac{\Delta t}{\tau^n_{i,j}}(\mathcal{E}_\mathrm{k}[\boldsymbol{\rho}^n_{i,j}] - [\mathcal{D}^n_{i,j} f^n_{i,j}]_\mathrm{k}), \end{aligned}$$

for $\mathrm{k} \in \mathcal{K}$ and $i,j = 1,\dots,i_{max},j_{max}$. For the second order scheme, the flux limiters (non differentiable) are kept explicit. The following δ matrix-form of the scheme is more adapted to computations

$$\left(\frac{I}{\Delta t} + T + R^n\right)\delta f^n = RHS^n, \tag{39}$$

where $\delta f^n = f^{n+1} - f^n$, I is the unit matrix, T is a matrix such that $(Tf^n)_{\mathrm{k},i,j} = \frac{1}{\Delta x}(\mathcal{F}^n_{\mathrm{k},i+\frac12,j} - \mathcal{F}^n_{\mathrm{k},i-\frac12,j}) + \frac{1}{\Delta y}(\mathcal{F}^n_{\mathrm{k},i,j+\frac12} - \mathcal{F}^n_{\mathrm{k},i,j-\frac12})$ with only the first order fluxes, R^n is such that $(R^n f^n)_{i,j} = \frac{1}{\tau^n_{i,j}}(f^n_{i,j} - \mathcal{D}^n_{i,j} f^n_{i,j})$, and

$$\begin{aligned} RHS^n_{\mathrm{k},i,j} \;=\; & -\frac{1}{\Delta x}(\mathcal{F}^n_{\mathrm{k},i+\frac12,j} - \mathcal{F}^n_{\mathrm{k},i-\frac12,j}) - \frac{1}{\Delta y}(\mathcal{F}^n_{\mathrm{k},i,j+\frac12} - \mathcal{F}^n_{\mathrm{k},i,j-\frac12}) \\ & + \frac{1}{\tau^n_{i,j}}(\mathcal{E}_\mathrm{k}[\boldsymbol{\rho}^n_{i,j}] - f^n_{\mathrm{k},i,j}) \end{aligned}$$

which contains the limiters for the second order scheme. The Jacobian $\mathcal{D}^n_{i,j}$ has the simple form

$$\mathcal{D}^n_{i,j}[\mathrm{k},\mathrm{k}'] = A^{-1}(\boldsymbol{\alpha}^n_{i,j}) : \boldsymbol{m}(v_\mathrm{k}) \otimes \boldsymbol{m}(v_{\mathrm{k}'})\mathcal{E}_\mathrm{k}[\boldsymbol{\rho}^n_{i,j}]\Delta v_x \Delta v_y \Delta v_z, \tag{40}$$

where $A(\boldsymbol{\alpha}^n_{i,j}) = \langle \boldsymbol{m} \otimes \boldsymbol{m} \exp(\boldsymbol{\alpha}^n_{i,j} \cdot \boldsymbol{m}) \rangle_{\mathcal{K}}$. A similar scheme can be derived for the BGK-ES model.

The particular structure of matrices T and R^n may be noted. If quantities $f^n_{\mathrm{k},i,j}$ are stored as $f^n = (f^n_{\mathrm{k}})_{\mathrm{k}\in\mathcal{K}}$ with $f^n_{\mathrm{k}} = (f^n_{\mathrm{k},i,j})$, then it can easily be seen (cf. figure 1) that T is a $N_v N_c \times N_v N_c$ block diagonal matrix with $N_c \times N_c$ pentadiagonal blocks T_{k} ($N_c = i_{max} \times j_{max}$ is the number of cells), and that R^n is a full matrix of diagonal blocks $R^n_{\mathrm{k},\mathrm{k}'}$. One can also note that if f^n_{k} is stored by i then by j, then the $(i,j)^{th}$ line of a block T_{k} is

$$[0,\dots,0,T_{\mathrm{k},i-1,j},0,\dots,0,T_{\mathrm{k},i,j-1},T_{\mathrm{k},i,j},T_{\mathrm{k},i,j+1},0,\dots,0,T_{\mathrm{k},i+1,j},0,\dots,0],$$

with

$$T_{\mathrm{k},i-1,j} = -\tfrac{1}{\Delta x} v_x^{k,+}, \quad T_{\mathrm{k},i,j-1} = -\tfrac{1}{\Delta y} v_y^{l,+},\ T_{\mathrm{k},i,j} = \tfrac{1}{\Delta x}|v_x^k| + \tfrac{1}{\Delta y}|v_y^l|,$$
$$T_{\mathrm{k},i,j+1} = \tfrac{1}{\Delta y} v_y^{l,-},\ T_{\mathrm{k},i+1,j} = \tfrac{1}{\Delta x} v_x^{k,-}.$$

The diagonal element of the $(i,j)^{th}$ line of a block $R^n_{\mathrm{k},\mathrm{k}'}$ is

$$\frac{1}{\tau^n_{i,j}}(\delta_{\mathrm{k},\mathrm{k}'} - \mathcal{D}^n_{i,j}[\mathrm{k},\mathrm{k}']),$$

where $\delta_{\mathrm{k},\mathrm{k}'}$ is the Kronecker symbol, and $\mathcal{D}^n_{i,j}[\mathrm{k},\mathrm{k}']$ is defined in (40). These sparse structures are naturally due to the fact that relaxation process in BGK equation is local in space but global in velocity, whereas transport process is numerically global in space but local in velocity.

REMARK 5.8. *As for the explicit scheme, a linearized implicit scheme can be derived for curvilinear meshes. This scheme can be written as in (39), but the elements of a bloc T_{k} depend on i and j; we have*

$$T_{\mathrm{k},i-1,j} = -\frac{1}{\Delta\xi}\left[v_{\mathrm{k}} \cdot \left(\frac{\nabla\xi}{J}\right)_{i-\frac{1}{2},j}\right]^+, \quad T_{\mathrm{k},i,j-1} = -\frac{1}{\Delta\eta}\left[v_{\mathrm{k}} \cdot \left(\frac{\nabla\eta}{J}\right)_{i,j-\frac{1}{2}}\right]^+,$$
$$T_{\mathrm{k},i,j} = \frac{1}{\Delta\xi}\left(\left[v_{\mathrm{k}} \cdot \left(\frac{\nabla\xi}{J}\right)_{i+\frac{1}{2},j}\right]^+ - \left[v_{\mathrm{k}} \cdot \left(\frac{\nabla\xi}{J}\right)_{i-\frac{1}{2},j}\right]^-\right)$$
$$+\frac{1}{\Delta\eta}\left(\left[v_{\mathrm{k}} \cdot \left(\frac{\nabla\eta}{J}\right)_{i,j+\frac{1}{2}}\right]^+ - \left[v_{\mathrm{k}} \cdot \left(\frac{\nabla\eta}{J}\right)_{i,j-\frac{1}{2}}\right]^-\right),$$
$$T_{\mathrm{k},i,j+1} = \frac{1}{\Delta\eta}\left[v_{\mathrm{k}} \cdot \left(\frac{\nabla\eta}{J}\right)_{i,j+\frac{1}{2}}\right]^-, \quad T_{\mathrm{k},i+1,j} = \frac{1}{\Delta\xi}\left[v_{\mathrm{k}} \cdot \left(\frac{\nabla\xi}{J}\right)_{i+\frac{1}{2},j}\right]^-.$$

5.2.2. Resolution of the linear system (39)

The linear system (39) to be solved at each iteration is very large ($N_v N_c \times N_v N_c$), and an iterative method well adapted to different sparse structures of the matrices may be used. We use here an algorithm based on a coupling between Jacobi and

Gauss-Seidel methods by using the storage of figure 1. First, R^n is separated into its block diagonal Δ^n and its block off-diagonal E^n, *i.e.* $R^n = \Delta^n - E^n$ (this is the Jacobi step). Then system (39) is equivalent to

$$\left(\frac{I}{\Delta t} + T + \Delta^n\right)\delta f^n = RHS^n + E^n \delta f^n.$$

Since the matrix of this linear system is block diagonal with pentadiagonal blocks $\frac{I}{\Delta t} + T_{\rm k} + \Delta^n_{\rm k}$, it is possible to use a line Gauss-Seidel method by setting $T_{\rm k} = M_{\rm k} - N_{\rm k}$. This gives the following algorithm:

ALGORITHM 1.

1. **set** $g^{(0)} = 0$,
2. **for** $p = 0, \ldots, P$, **solve**

$$\left(\frac{I}{\Delta t} + M_{\rm k} + \Delta^n_{\rm k}\right) g^{(p+1)}_{\rm k} = RHS^n_{\rm k} + N_{\rm k} g^{(p)}_{\rm k} + [E^n g^{(p)}]_{\rm k}, \quad {\rm k} \in \mathcal{K} \tag{41}$$

3. **set** $\delta f^n = g^{(P+1)}$.

The linear systems (41) may easily and exactly be solved by successive LU decompositions of tridiagonal matrices of $\mathbf{R}^{i_{max}\times i_{max}}$ or $\mathbf{R}^{j_{max}\times j_{max}}$. Note that calculating the product $E^n g$ is not very expensive because the blocks of E^n are diagonal. In fact we have

$$[E^n g]_{{\rm k},i,j} = \frac{1}{\tau^n_{i,j}} A^{-1}(\boldsymbol{\alpha}^n_{i,j}) \boldsymbol{m}(v_{\rm k}) \mathcal{E}_{\rm k}[\boldsymbol{\rho}^n_{i,j}] \cdot \Big(\langle \boldsymbol{m} g_{i,j} \rangle_{\mathcal{K}} - \boldsymbol{m}(v_{\rm k}) g_{{\rm k},i,j} \Delta v_x \Delta v_y \Delta v_z \Big).$$

It is thus sufficient to compute $A^{-1}(\boldsymbol{\alpha}^n_{i,j}) \boldsymbol{m}(v_{\rm k}) \mathcal{E}_{\rm k}[\boldsymbol{\rho}^n_{i,j}]$ at the beginning of the algorithm (a local computation in k and i,j), then to compute $\langle \boldsymbol{m} g_{i,j} \rangle_{\mathcal{K}}$ on each cell (which is local in i,j), and finally to form the dot product. The computation of $E^n g$ is thus local in i,j, and hence completely parallelizable; its cost is in $O(N_c N_v)$.

It is well known in CFD that since only a few iterations are needed to have the external process converge (the loop in n), it is not useful to carry on an algorithm like the previous one at convergence. The cost of our implicit scheme is then in $O(P N_v N_c)$ where $P = 2$ or 3, which is confirmed by numerical experiments (see [26]).

5.3. Computation of $\boldsymbol{\alpha}^n_{i,j}$

The nonlinear set of equations (36) may be solved by the following Newton algorithm, where F is defined by $F(\boldsymbol{\beta}) = \langle \boldsymbol{m} \exp(\boldsymbol{\beta} \cdot \boldsymbol{m}) \rangle_{\mathcal{K}} - \boldsymbol{\rho}^n_{i,j}$.

ALGORITHM 2.

1. **set** $\boldsymbol{\alpha}^{(0)} \in \mathbf{R}^4$,
2. **solve** the linear system $F'(\boldsymbol{\alpha}^{(r)}) \boldsymbol{\alpha}^{(r+1)} = \boldsymbol{\alpha}^{(r)} - F(\boldsymbol{\alpha}^{(r)})$
   until a stop criterion is satisfied,
3. **set** $\boldsymbol{\alpha}^n_{i,j} = \boldsymbol{\alpha}^{(r)}$.

Such an algorithm requires almost $12N_v$ operations by iteration r and by cell (i,j) and is thus in $O(N_cN_v)$. For most cases we have tested, this algorithm is robust enough, if the initial datum is wisely chosen (cf. below). However, a back-tracking linesearch algorithm may be employed if the matrix $F'(\boldsymbol{\alpha}^{(r)}) = \langle \boldsymbol{m} \otimes \boldsymbol{m} \exp(\boldsymbol{\alpha}^{(r)} \cdot \boldsymbol{m}) \rangle_{\mathcal{K}}$ is too much ill-conditioned. This may happen when the velocity of the flow is very high, since the last element of $\boldsymbol{m}(v_{\mathrm{k}}) \otimes \boldsymbol{m}(v_{\mathrm{k}})$ is $|v_{\mathrm{k}}|^4$, whereas the first one is always 1. For the initial condition $\boldsymbol{\alpha}^{(0)}$, we use the parameter $\boldsymbol{\alpha}$ of the continuous equation (2) at the beginning of the computation. Then, when the flow is almost stabilized, we take $\boldsymbol{\alpha}^{(0)} = \boldsymbol{\alpha}_{i,j}^{n-1}$ computed at the previous global iteration. With this choice, the algorithm converges rapidly - only one iteration is needed for most cases tested. The same algorithm is used to compute the vector $\vec{\alpha}_{i,j}^n$ which defines the discrete Gaussian $\mathcal{G}_{\mathcal{K}}[f_{i,j}^n]$ of the BGK-ES model.

5.4. Axisymmetric flows

Consider a discrete-velocity model for the conservative form equation, as given by (34). The explicit scheme of section 5.1 can now be applied to this model

$$\begin{aligned} f_{\mathrm{k},i,j}^{n+1} = f_{\mathrm{k},i,j}^n \; - \; & \frac{\Delta t}{\Delta x}(\mathcal{F}_{\mathrm{k},i+\frac{1}{2},j}^n - \mathcal{F}_{\mathrm{k},i-\frac{1}{2},j}^n) - \frac{\Delta t}{r_j \Delta r}(r_{j+\frac{1}{2}}\mathcal{F}_{\mathrm{k},i,j+\frac{1}{2}}^n - r_{j-\frac{1}{2}}\mathcal{F}_{\mathrm{k},i,j-\frac{1}{2}}^n) \\ + \; & \frac{\Delta t}{\tau_{i,j}^n}(\mathcal{E}_{\mathrm{k}}[\boldsymbol{\rho}_{i,j}^n] - f_{\mathrm{k},i,j}^n) + \Delta t \frac{\zeta_l}{r_j} D(\sin\omega f_{k,l,i,j}^n)_q. \end{aligned}$$

Note that owing to the cell-centered approach, the radius r_j is always strictly positive, even near the symmetry axes (where $r_j = \frac{1}{2}\Delta r$).

We can prove that if the operator D has the properties mentioned in section 4, then this explicit scheme is also positive, conservative, and entropic. Note that the only difference with the Cartesian case is the presence of the term $\Delta t \frac{\zeta_l}{r_j} D(\sin\omega f_{k,l,i,j}^n)_q$. For the linearized implicit scheme, the opposite of this term can be rewritten under a matrix-vector product $A^n f^n$ where A^n is a full matrix of diagonal blocks. Then we have the following scheme

$$\left(\frac{I}{\Delta t} + T + R^n + A^n\right)\delta f^n = RHS^n.$$

The Jacobi-Gauss-Seidel algorithm 0 can be applied to this linear system. As for R^n, we split A^n into its diagonal part Δ_{A^n} and its off-diagonal part $-E_{A^n}$ in the Jacobi step of the algorithm. The algorithm is now

Algorithm 3.

1. **set** $g^{(0)} = 0$,
2. **for** $p = 0, \ldots, P$ and $\mathrm{k} \in \mathcal{K}$, **solve**

$$\left(\frac{I}{\Delta t} + M_{\mathrm{k}} + \Delta_{\mathrm{k}}^n + [\Delta_{A^n}]_{\mathrm{k}}\right) g_{\mathrm{k}}^{(p+1)} = RHS_{\mathrm{k}}^n + N_{\mathrm{k}} g_{\mathrm{k}}^{(p)} + [(E^n + E_{A^n})g^{(p)}]_{\mathrm{k}},$$

3. **set** $\delta f^n = g^{(P+1)}$.

For instance, with the operator T-UCE, we have

$$[\Delta_{A^n}]_{\mathrm{k},i,j} = -\frac{\zeta_l}{r_j 2\sin\frac{\Delta\omega}{2}}\Big((\sin\omega_{q+\frac{1}{2}})^+ - (\sin\omega_{q-\frac{1}{2}})^-\Big),$$
$$[E_{A^n} f^n]_{\mathrm{k},i,j} = \frac{\zeta_l}{r_j 2\sin\frac{\Delta\omega}{2}}\Big((\sin\omega_{q+\frac{1}{2}})^+ f^n_{k,l,q+1,i,j} - (\sin\omega_{q-\frac{1}{2}})^- f^n_{k,l,q-1,i,j}\Big).$$

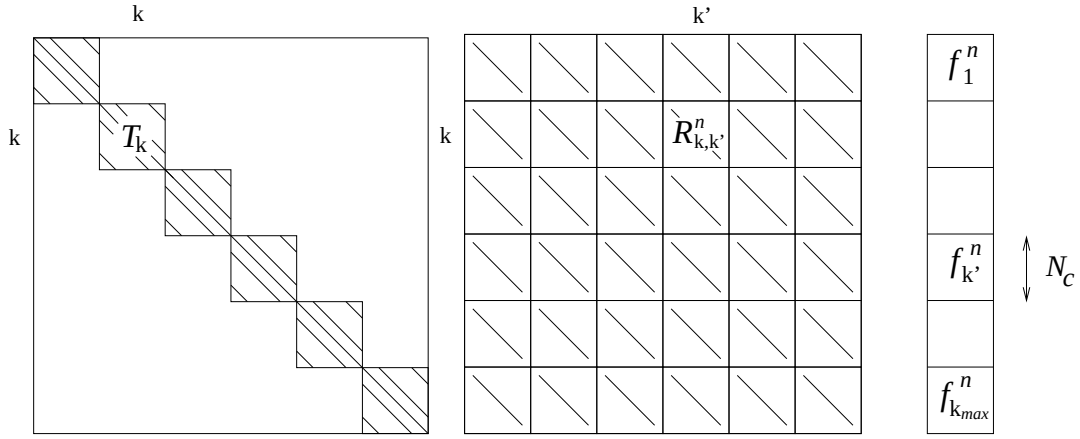

FIG. 1. Matrices T and R^n, and corresponding storage of vector f^n.

6. NUMERICAL RESULTS

We present numerical tests for plane and axisymmetric flows. For plane flows, the improvement of the results due tot the BGK-ES model is shown. We also show test cases where our implicit deterministic method is a relevant alternative to DSMC. For axisymmetric flows, the different discretizations of Sec. 4 are compared on 1D cases. We also present an application of these schemes to an axisymmetric flow around a sphere.

Except in some cases, the linearized implicit scheme of second order is used in all the computations, with a CFL number of 10000 (*i.e.* Δt is 10000 times the explicit time step). The criterion used to determine whether the flow has reached steady state is the reduction of the quadratic global residual $\frac{1}{\Delta t}(\sum_{k,i,j} |RHS^n_{k,i,j}|^2)^{\frac{1}{2}}$ by a factor of 10^5.

Numerically, all the boundary conditions (gas-surface, symmetry axes, etc.) are treated by a classical ghost cell technique (see [37]. For instance, incident molecules in a boundary cell of indexes $(i, j = 1)$ are supposed to be re-emitted by the wall from a ghost cell of indexes $(i, 0)$. This cell is the mirror cell of $(i, 1)$ with respect to the wall. The diffuse reflection (13) is then modeled by

$$f^n_{\mathrm{k},i,0} = \phi_{i,1}\, \mathcal{E}_{\mathrm{k}}[\boldsymbol{\rho}_w], \quad v_{\mathrm{k}} \cdot n_{i,1} > 0,$$

where $\phi_{i,1}$ is determined so as to avoid a mass flux across the wall, *i.e.* between cells $(i, 0)$ and $(i, 1)$. Relation (14) gives

$$\phi_{i,1} = -\frac{\sum_{v_{\mathrm{k}} \cdot n_{i,1} < 0} v_{\mathrm{k}} \cdot n_{i,1}\, f^n_{k,i,1} \Delta v_x \Delta v_y \Delta v_z}{\sum_{v_{\mathrm{k}} \cdot n_{i,1} > 0} v_{\mathrm{k}} \cdot n_{i,1}\, \mathcal{E}_{\mathrm{k}}[\boldsymbol{\rho}_w] \Delta v_x \Delta v_y \Delta v_z}$$

Moreover, relation (6), where δ is given for each gas in [7], is used to compute the relaxation time of the model. As explained in section 2, this depends on the molecular interaction potential. For each test case, we specify which potential is used among VHS, Hard-Sphere, and Maxwellian potentials. In each comparison, a unique potential is used for the three methods (BGK, BGK-ES, DSMC).

Note that the velocity grid is appropriately chosen for each case. Since the same grid is used in each point of space, it should be large and precise enough to correctly describe the flow (*i.e.* the distributions everywhere in the space domain). Then the bounds are given by a combination between the maximum macroscopic velocity and temperature of the flow ($\max_{\mathrm{x}}(u + c\sqrt{RT})$, where we take $c = 4$). The step of the grid is given by the smallest temperature (*i.e.* $\Delta v = \min_{\mathrm{x}} \sqrt{RT}$). These quantities may be estimated by two methods. First in some cases, they are given by the data, *e.g* velocity and temperature at infinity and wall temperature. But for more "extreme" flows, the maximum temperature is much greater than these data. Then in that cases, we make a converged Navier-Stokes computation, and the converged values of the macroscopic velocity and temperature are sufficient for defining a correct velocity grid.

Finally, note that all the tests presented here have been computed on the single processor of the IBM-SP2 (120 MHz - 512 Mo).

6.1. Plane flows

6.1.1. Compression ramp

Here our method for BGK and BGK-ES equations is compared to the DSMC method, which simulates the Boltzmann equation with the code of J.-C. Lengrand [23], and to the Navier-Stokes equations (without slip condition). We study a supersonic flow past a flat plate of $5\,cm$ followed by a compression ramp of $10°$. The gas is air, and the parameters of the flow are $\rho_\infty = 1.288\,10^{-4}\,kg.m^{-3}, T_\infty = 72.2\,K, M_\infty = 3.67$, for the density, temperature and Mach number. The wall temperature is $72.2\,K$. The molecular mass is $4.815\,10^{-26}\,kg$ and the viscosity exponent δ is 0.77 (VHS model). This gives a Knudsen number of $6.7\,10^{-3}$ at infinity. For the four methods, we use the same mesh of 70×70 cells. For BGK and BGK-ES, the velocity grid has $13 \times 11 \times 11$ points with bounds $[-1500, 1500] \times [-1200, 1200] \times [-1200, 1200]$.

For the BGK model, the computation takes 260 iterations and 42 hours CPU. For BGK-ES, it takes 564 iterations and 60 h CPU. For the DSMC, the computation takes 8000 iterations and 46 h CPU. We used 2600 samples and an average of 20 particles per cell, with a time step of $5\,10^{-7}\,s$. The Navier-Stokes computation takes less than 10 min CPU.

The contours of density and temperature are plotted in figure 2 for the four methods. The results obtained with BGK, BGK-ES and DSMC are very close, and this can be seen more clearly in figure 3 where the distribution of temperature following three vertical lines $x = 2.5, 5, 7.5\ cm$ is shown. One can only note a difference near the wall where BGK-ES is more accurate than BGK. The influence of the Prandtl number is thus clear. On the other hand, Navier-Stokes equations give very poor results at the beginning of the plate and within the shock. An explanation is that the local Knudsen number (see [7]) at the leading edge is 0.13, which is beyond the validity range of Navier-Stokes equations. In fact, Bird notices in [7] that the error in Navier-Stokes results is significant in the regions of the flow where the local Knudsen number exceeds 0.1. For the DSMC, note the noise induced by the stochasticity of the method. Also, it is apparent that the results of the DSMC are inaccurate in the small region in front of the downstream boundary. This is a direct consequence of a defect in the boundary conditions (see [11]). Although the CPU times of BGK and DSMC are provided for this case, a fair comparison of computational speeds of the two methods is not easy because their criteria of convergence are very different. For instance, making more samples to decrease the noise in DSMC results can strongly increase the CPU time of this method.

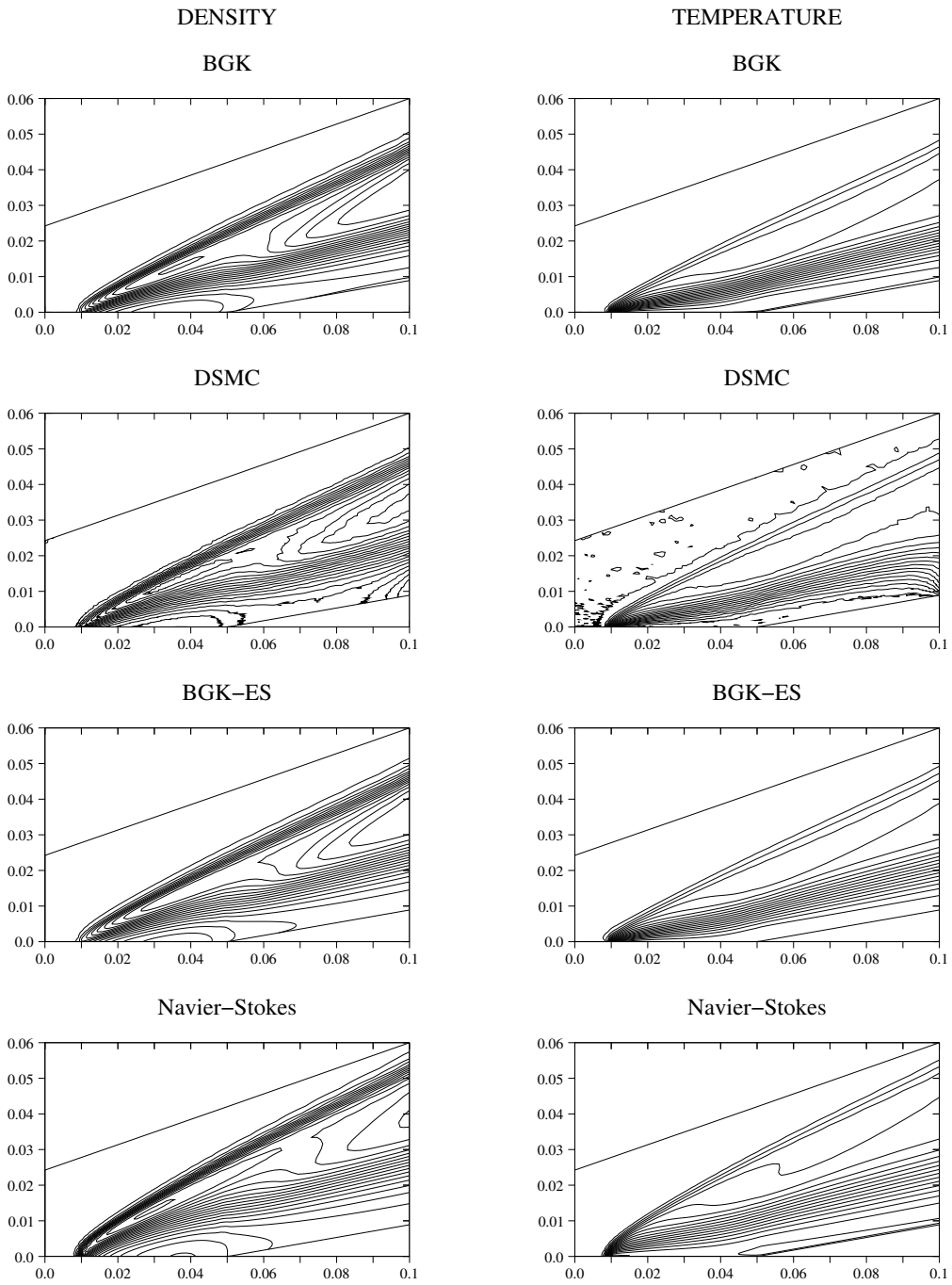

FIG. 2. Compression ramp: density (left) and temperature (right) for BGK, DSMC, BGK-ES and Navier-Stokes.

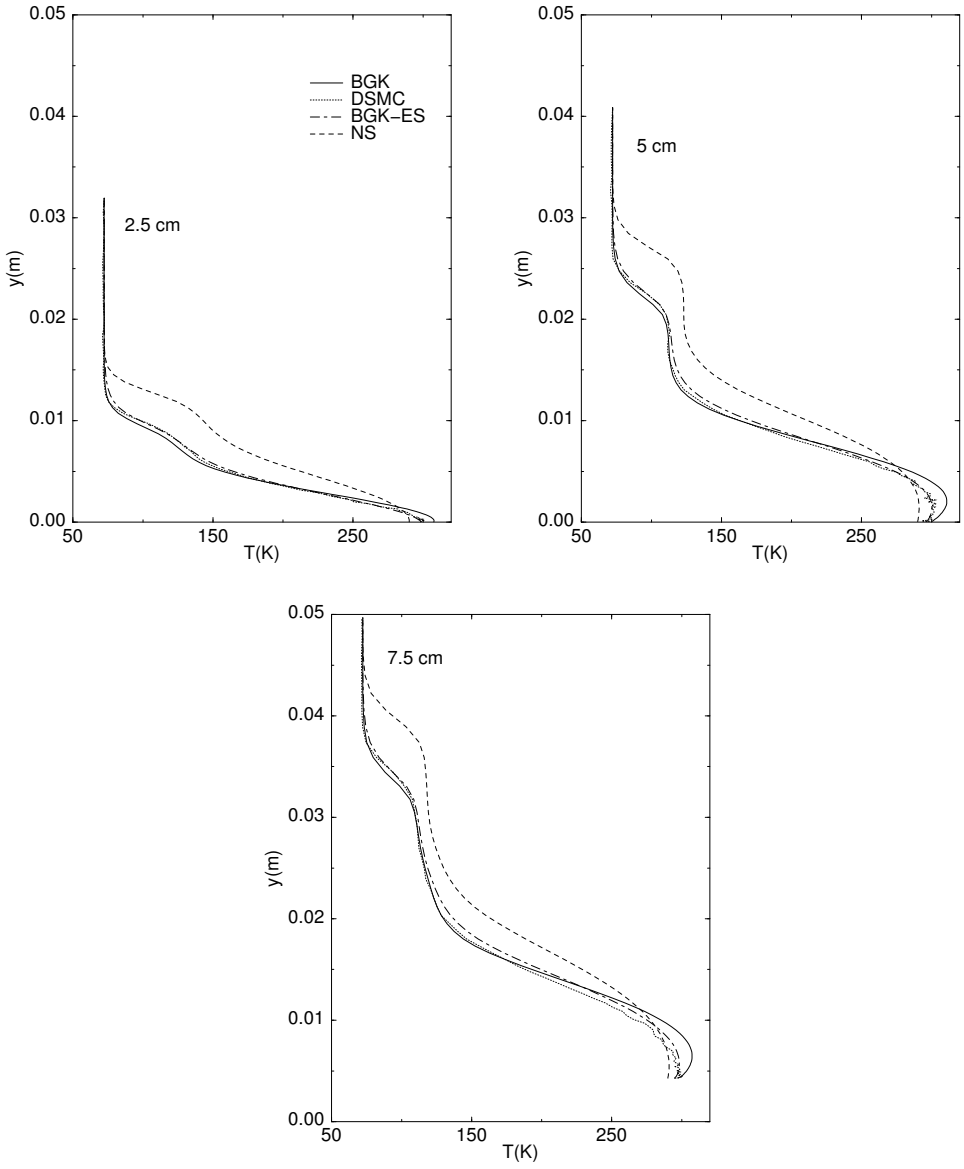

FIG. 3. Compression ramp: temperature distribution along three vertical lines ($x = 2.5$, 5, 7.5 cm) for BGK, DSMC, BGK-ES, and Navier-Stokes.

6.1.2. Recirculation

We want to prove that it is relevant to use BGK for flows with a recirculation zone. It is well known that particle methods like DSMC have some difficulties to converge in these situations. A problem is that, due to the low velocity of the flow in the recirculation, a large number of iterations may be needed to reach steady state. Moreover, the density is often very low in such a zone, which implies that after a long time, particle methods have not enough representative molecules to correctly describe the gas.

Here we consider a supersonic plane flow past a cylinder of radius $1\,m$. The parameters of the flow are $\rho_\infty = 0.31696\,10^{-5}\,kg.m^{-3}, T_\infty = 249\,K, M_\infty = 4$, for the density, temperature and Mach number. The wall temperature is $293\,K$. The molecular mass is $0.663\,10^{-25}\,kg$ and the viscosity exponent δ is 0.5 (Hard-Sphere model). This gives a Knudsen number of 0.0358 at infinity. These characteristics correspond to an atmospheric flow at 90 km of altitude (but here, the gas is argon). We use a mesh of 49×60 cells, and a velocity grid of bounds $[-2562, 2562] \times [-2462, 2462] \times [-2303, 2303]$ with 11 points in each direction. We test our BGK method and the DSMC on this mesh. For DSMC, with 20 particles per cell, the steady state is reached after 250 iterations with a time step of $1.\,10^{-4}\,s$. After, we used 2500 samples (each 3 times steps) to compute macroscopic values. Note that the mesh respects the criterion of cell size lower than the mean-free-path only near the wall. Thus one can expect that DSMC results will not be very accurate.

For BGK, the computation takes 1167 iterations and 90 h CPU. The DSMC computation takes 50 h CPU, which is shorter than for BGK. The total number of molecules in the flow is stabilized at the end of the computation, which proves that the flow has reached steady-state. However, the cells in the recirculation zone contain between one and five molecules only, which is clearly not sufficient to correctly describe the gas. This problem is also observed in figure 4, because the recirculation zone (visible on the zoom on velocity field) is poorly described by DSMC, contrary to our method. In addition, we observe that the time step is too large in the shock since it is ten times as large as the inverse collision frequency. Finally note the noise on density contours obtained with DSMC.

Consequently, whereas BGK is more expensive than DSMC on this test case, our method appears to be more accurate. Note that with DSMC, a smaller time step and almost five times as many molecules as in this computation would be necessary to obtain more correct results. Then the CPU time of DSMC would be greater than the cost of BGK.

Also note that contrary to DSMC, the parameters of our method do not need to be adapted if there is a recirculation zone. The resolution of the velocity grid is not affected by this phenomenon, contrary to the number of molecules of DSMC. This suggests that our method is simpler to use.

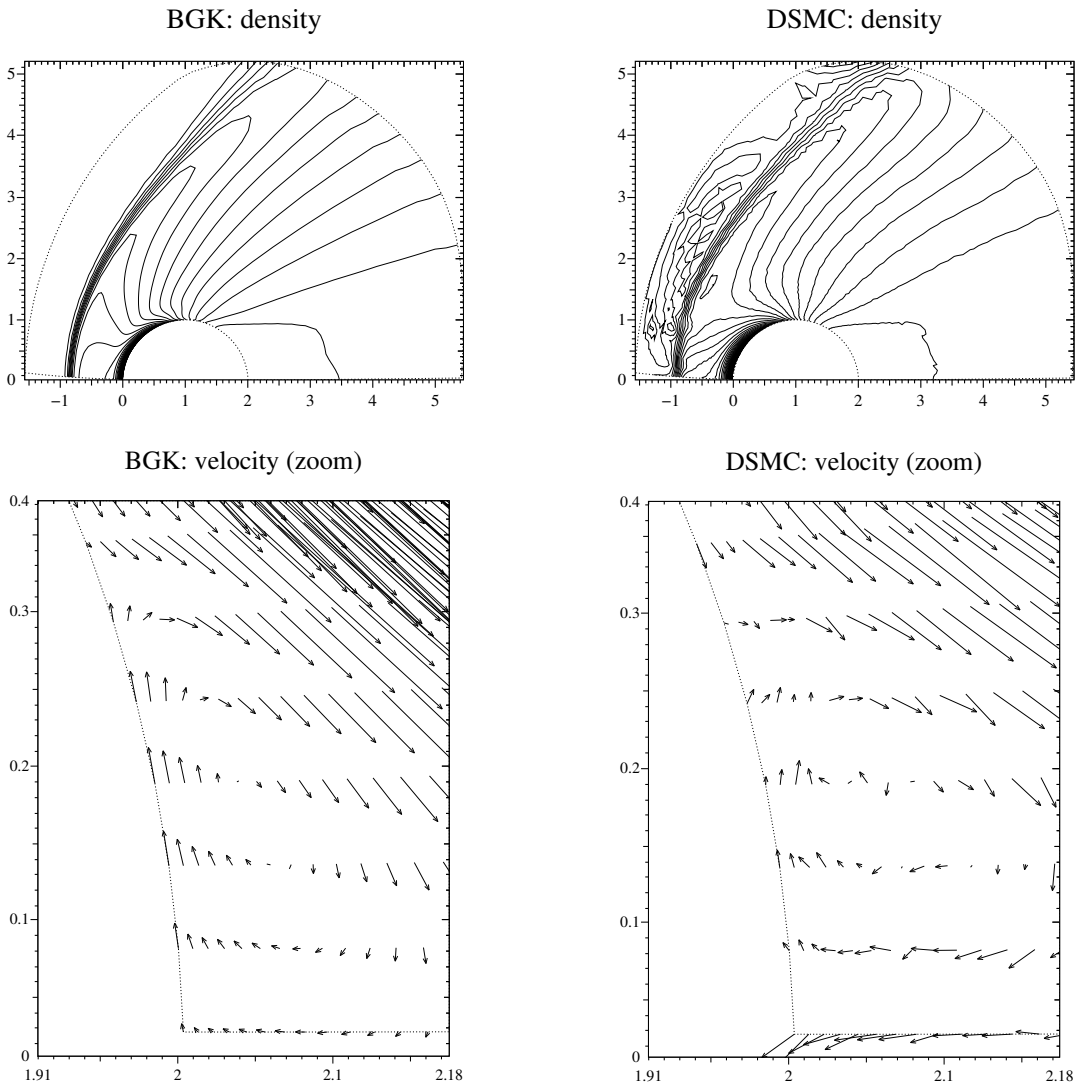

FIG. 4. Recirculation behind a cylinder. Comparison between BGK and DSMC: density (up) and velocity field in the recirculation (down).

6.1.3. Hypersonic flow

We present this case for testing the robustness of our method on hypersonic flows (and particularly the Newton algorithm and the linear solver). This is an hypersonic flow at Mach 18.3 without incidence on a flat plate of length $10\,cm$, width $0.5\,cm$ and an angle of length $1.4\,cm$ at the leading edge. The parameters of the flow are: $\rho_\infty = 5.19\,10^{-5}\,kg.m^{-3}, T_\infty = 13.6\,K, M_\infty = 18.3$, for the density, temperature and Mach number. The molecular mass is $4.65\,10^{-26}\,kg$ and the viscosity exponent is 0.5 (Hard-Sphere model). This gives a Knudsen number of $1.4\,10^{-2}$ at infinity. This case has been studied by Andriès-Bourgat-Le Tallec-Perthame in [1] with a Monte-Carlo-like code which simulates Boltzmann, BGK, and BGK-ES equations (see also [10]).

For BGK, we use a mesh of 75×29 cells in tangent and orthogonal directions to the plate. This is very coarse compared to the mesh of [1] which has almost 180×180 cells. A Navier-Stokes computation gives a velocity grid of bounds $[-2300, 2300] \times [-1600, 1600] \times [-1300, 1300]$ with $31 \times 29 \times 27$ velocities. Such a grid would lead to very long computations, then we only take $21 \times 21 \times 21$ velocities. The computation takes 140 iterations and 36 h CPU. We observe that the code succeeds in computing such a violent flow. This confirms the robustness of the implicit scheme and of the Newton algorithm.

Our results are plotted in figures 5 and 6. First, we note that our results are globally quite close to that of [1], whereas our mesh is much less refined (because the deterministic resolution of BGK does not require a mesh as fine as DSMC).

One can have an idea of the kinetic non-equilibrium near the leading edge by noting that the local Knudsen number is 0.5, and by plotting the reduced distribution function $F(v_x, v_y) = \int f(v_x, v_y, v_z)\, dv_z$ (see figure 6). One can clearly see the half-Maxwellian of the wall centered on $u_x = 0$, and the Maxwellian of the upstream flow, centered on the upstream velocity $u_x = 1500$. As the wall temperature is greater than the upstream one, the half-Maxwellian is more spread.

We want to emphasize that the conservation and entropy properties of our discrete-velocity model are essential in the fact that we need only 21^3 discrete velocities to reach steady state. For comparison, note that in [36], for a case at Mach 12 (instead of 18.3 here), it is needed more than 70 discrete velocities in each direction with a non-conservative discretization.

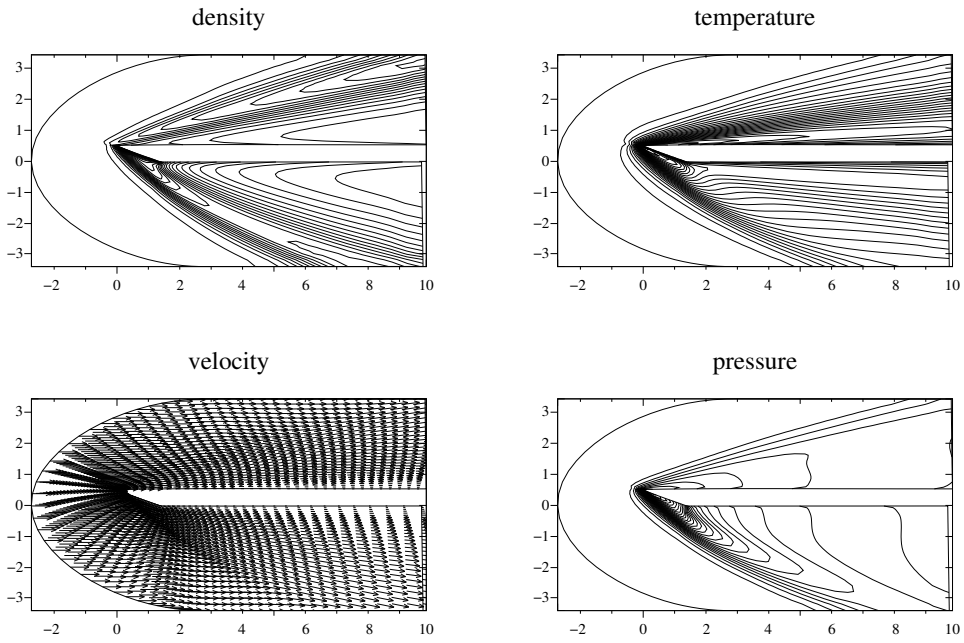

FIG. 5. Contours and velocity field for hypersonic flow past a flat plate.

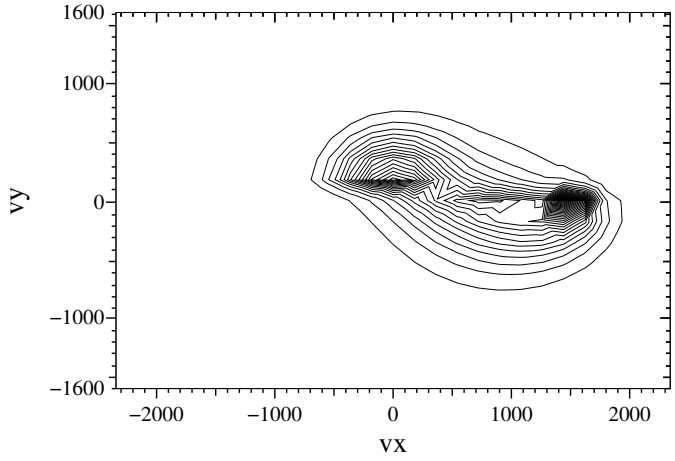

FIG. 6. Reduced distribution function $F(v_x, v_y)$ at the leading edge of the flat plate. Note the half-Maxwellian of the wall centered on $v_x = 0$, and the Maxwellian of the upstream flow, centered on the upstream velocity $u_x = 1500$.

6.2. Axisymmetric flows

6.2.1. 1D flow

We consider a gas between two coaxial cylinders. The large cylinder rotates at a constant velocity and the small one is stationary. Therefore the flow depends only on the radius r. This case has the advantage of being computable either by a 2D plane method or by a 1D axisymmetric method (cf. figure 7). Moreover, the total mass of the gas is constant, then it is a good case for testing the conservation properties of our schemes. The parameters of the flow are the following: the gas is argon of molecular mass $0.663\,10^{-25}$ kg and of viscosity exponent $\delta = 0.5$ (Hard-Sphere model). The flow is initially at temperature 300 K and of density $0.1247\,10^{-5}\,kg.m^{-3}$. The large cylinder rotates a constant speed of $106\,m.s^{-1}$, and the two cylinders have a temperature of 300 K. They have radius $R_1 = 1\,m$ and $R_2 = 2\,m$. This gives a Knudsen number based on R_1 of 0.1. For the 2D plane computation in the (y, z)-plane, the mesh has 22×20 cells in φ and r directions (cf. figure 7). The velocity grid has 9^3 velocities and bounds $[-1000, 1000]^3$. For the 1D axisymmetric computations, we use a mesh of 20 cells in r direction and a velocity grid of $9 \times 6 \times 18$ points in (v_x, ζ, ω)-directions.

For plane and axisymmetric computations we use the explicit scheme, in order to plot the total mass during the unstationary part of the flow (see figure 8). First we observe that the upwind non-conservative schemes (U2NCE, T-U2NCE and UNCE) do not conserve the total mass at all: $M(t)$ rapidly decreases to 0. Thus the trigonometric correction T-UNCE of UNCE appears to be essential. For the second order centered non-conservative scheme CNCE, the mass is not conserved, but it changes only by 0.01% between the initial time and the steady state. For all the conservative schemes (UCE, T-UCE, CCE, T-CCE, T-CNCE, T-UNCE), the total mass is perfectly constant. Note that for the 2D plane computation the total mass is slightly decreasing, whereas the scheme is theoretically conservative. This is a consequence of the approximation of the curved boundaries with the curvilinear mesh.

At steady state, we also plot the tangential velocity and the density for all our schemes (figure 9), except for UNCE, U2NCE, T-U2NCE that give totally incorrect results (they cannot be plotted on the same scale). This is not surprising, since these schemes satisfy the conservation laws only up to the first order (see sections 4.3 and 4.6). Considering the results of the 2D plane computation as the reference curves, we observe that second order axisymmetric schemes (in velocity) are much more accurate than the others (CCE, T-CCE, CNCE, T-CNCE). Moreover, there is only a small difference between the schemes and their trigonometric corrections, except for CCE. Also note that the trigonometric correction T-UNCE of UNCE gives very poor results, but however more accurate that UNCE itself. The reason is that T-UNCE is conservative, as opposed to UNCE, but does not preserve uniform flows.

If the number of points is increased from 18 to 60 in ω-direction of the velocity grid, then we observe that the difference between trigonometric corrections and basic schemes is smaller. The first order schemes are closer to second order schemes, and all the axisymmetric results are closer to plane results. Consequently, it is clear that axisymmetric computations require a more precise velocity discretization than plane computations. This is probably due to the fact that in axisymmetric case,

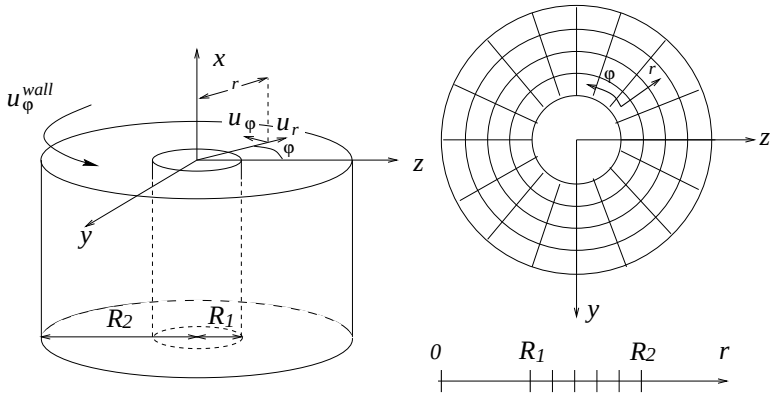

FIG. 7. Geometry of the flow between two cylinders (left), 2D plane mesh (top) and 1D axisymmetric mesh (bottom).

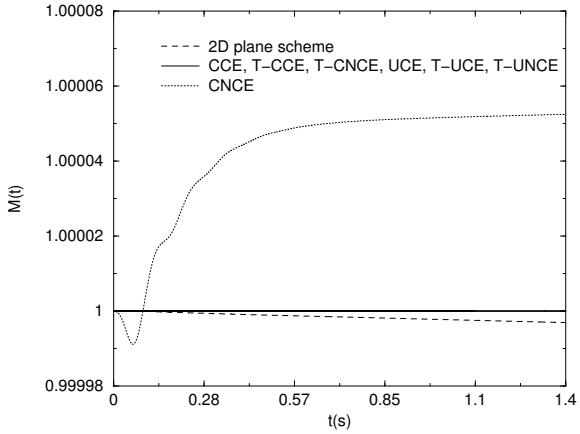

FIG. 8. Total mass $M(t)$ (normalized to 1) of the gas between two coaxial cylinders: schemes U2NCE, T-U2NCE, UNCE are not plotted here since $M(t)$ rapidly decreases to 0.

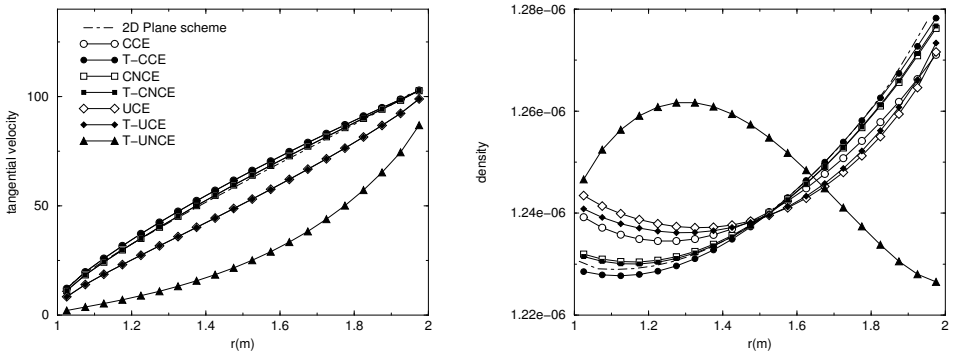

FIG. 9. Tangential velocity (left) and density (right) of the gas between two coaxial cylinders.

a velocity derivative of f must be approximated. In plane computations, only an approximation of the moments of f is needed, *i.e.* integrals on velocity space, which requires a less precise discretization. Finally, note that whereas the second order schemes do not theoretically preserve the positivity of f, this does not affect our results for this test-case.

For testing our implicit schemes, we use a slightly different test-case, taken from Sone et al. [33]. Here the only difference with the previous case is that the boundary conditions are now evaporation-condensation conditions. This means that at the surface of the cylinders, the distribution function is completely prescribed. Consequently, there is a mass flux across the boundaries, and the total mass is no longer conserved. Thus we can expect that conservation properties are less crucial here. On the small cylinder, the pressure is set to 0.0708, and to 0.0779 on the large cylinder, with the same temperature as previously. We plot the results for the tangential velocity and the temperature (figure 10), normalized by the parameters of the small cylinder (see [33]). The plane results are very close to that of [33]. For axisymmetric results, we found the same hierarchy between the schemes as in the previous test-case. The difference is that here, upwind non-conservative schemes (UNCE, U2NCE, T-U2NCE) give correct results. Moreover if the number of points ω_q is increased as previously (from 18 to 60), we observe that second order centered schemes become very unstable, and the computation stops. Consequently, despite their high accuracy, these schemes lack robustness.

This short study proves that the trigonometric second order centered schemes have the highest accuracy. Among these schemes, there is no significant difference between discretizations of the conservative and non-conservative form equations (T-CCE and T-CNCE). However, as it is proved with the last test case, these schemes lack robustness. Therefore, the best compromise between robustness and accuracy is the scheme T-UCE, which has numerous strong properties (see table 1).

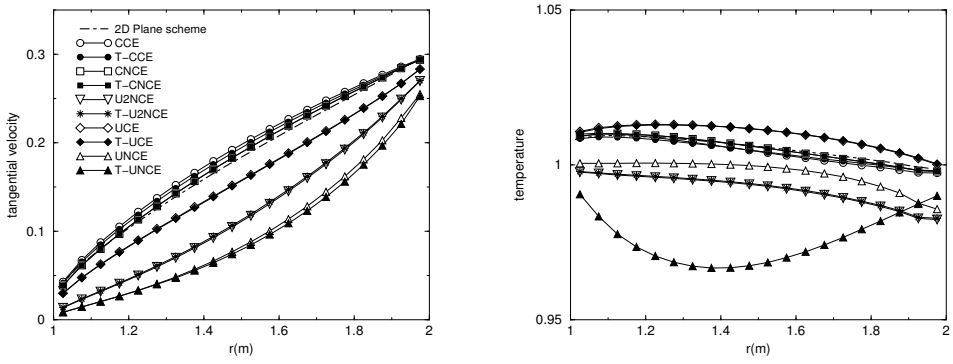

FIG. 10. Nondimensional tangential velocity $u_\varphi/\sqrt{2RT_1}$ (left) and temperature T/T_1(right) for the evaporation-condensation problem between two coaxial cylinders, where T_1 is the temperature of the small cylinder (case taken from [33]).

6.2.2. 2D supersonic flow past a sphere

In this test, we advance the validation of our method for solving the axisymmetric BGK equation. We consider a flow past a sphere of radius $0.1\,m$, with the parameters of an atmospheric flow at 90 km of altitude: $\rho_\infty = 0.317\,10^{-5}\,kg.m^{-3}, T_\infty = 249\,K, M_\infty = 5$, for the density, temperature and Mach number. The molecular mass is $0.663\,10^{-25}\,kg$ and the viscosity exponent is 0.81 (VHS model). This gives a Knudsen number of 0.236 at infinity.

For BGK, we use a mesh of 60×50 cells in tangential and orthogonal directions. The computational domain is restricted to the upstream flow, we have neglected the influence of the flow downstream from the sphere. The velocity grid has $11 \times 9 \times 21$ points in (v_x, ζ, ω) directions. Since the distribution function is even in ω, this variable is in $[0, \pi]$. The bounds of the grid for v_x and ζ are $[-2300, 2300] \times [0, 2000]$. The velocity discretization of the transport operator uses the T-UCE scheme, which has been proved in section 6.2.1 to be the best compromise between accuracy and robustness. The computation takes 137 iterations and 31 h CPU.

For the DSMC, we use the same mesh. Since the size of the cells is greater than the mean-free-path, one cannot expect accurate results. The parameters of the method are: 20 particles per cell, with a time step of $2\,10^{-6}\,s$. After 136 iterations we make 500 samples (one every three time steps). The maximum simulation time is reached in 1631 iterations and 18 h CPU. Therefore, the CPU time is lower than for BGK, but it would be much longer to obtain more accurate results. A Navier-Stokes computation (without slip condition) is also made.

The results are shown in figures 11 and 12. The noisy contours obtained with DSMC are not surprising (figure 11). We also note that BGK contours are oscillating in the tail of the shock. This phenomenon also arises with Navier-Stokes results although it is less visible. This is a classical problem of structured meshes, which is due to the numerical viscosity of the scheme, because the streamlines are not aligned with the mesh. However, the results of BGK and DSMC are quite close, which is not true for Navier-Stokes.

In figure 12, we plot density, temperature, and pressure profiles as functions of the radius r along two lines orthogonal to the wall. One is the symmetry axis, the other one is at 45° of this axis. For the first line, DSMC and BGK curves are quite close, except near the wall where there is a difference of approximately 20% for the temperature and the density. However, note that the difference between DSMC and Navier-Stokes is much larger, especially for the temperature. For the line at 45°, DSMC and BGK are strikingly close. At the contrary, we note a large difference between DSMC and Navier-Stokes. This is not surprising, since the local Knudsen number is found to be 0.6 in this zone. For instance, there is a difference of nearly 50% for the temperature in the shock ($r = 0.025\,m$).

One can estimate the gain obtained by using an axisymmetric computation instead of a full 3D computation. For estimating the CPU cost of a 3D computation, we have computed the same flow in 2D plane geometry, with a cylinder instead of a sphere, and with the same number of cells. A Cartesian computation requires a less precise velocity grid, then we use $11 \times 11 \times 11$ discrete velocities (this is almost a half as many discrete velocities as in the axisymmetric computation). The computation takes 194 iterations and 22 h CPU, which is of course faster than the axisymmetric case. For a 3D computation, assume that we would use 50 cells in

z-direction. Since our algorithms have a linear complexity, then we can assume that the 3D computation would be 50 times as long as the 2D plane case, which yields 1100 h CPU. This must be compared to the 31 h CPU for the same result with the axisymmetric computation. This is clear that despite the high cost of the discretization in ω, the 2D axisymmetric method is much less expensive than a full 3D computation.

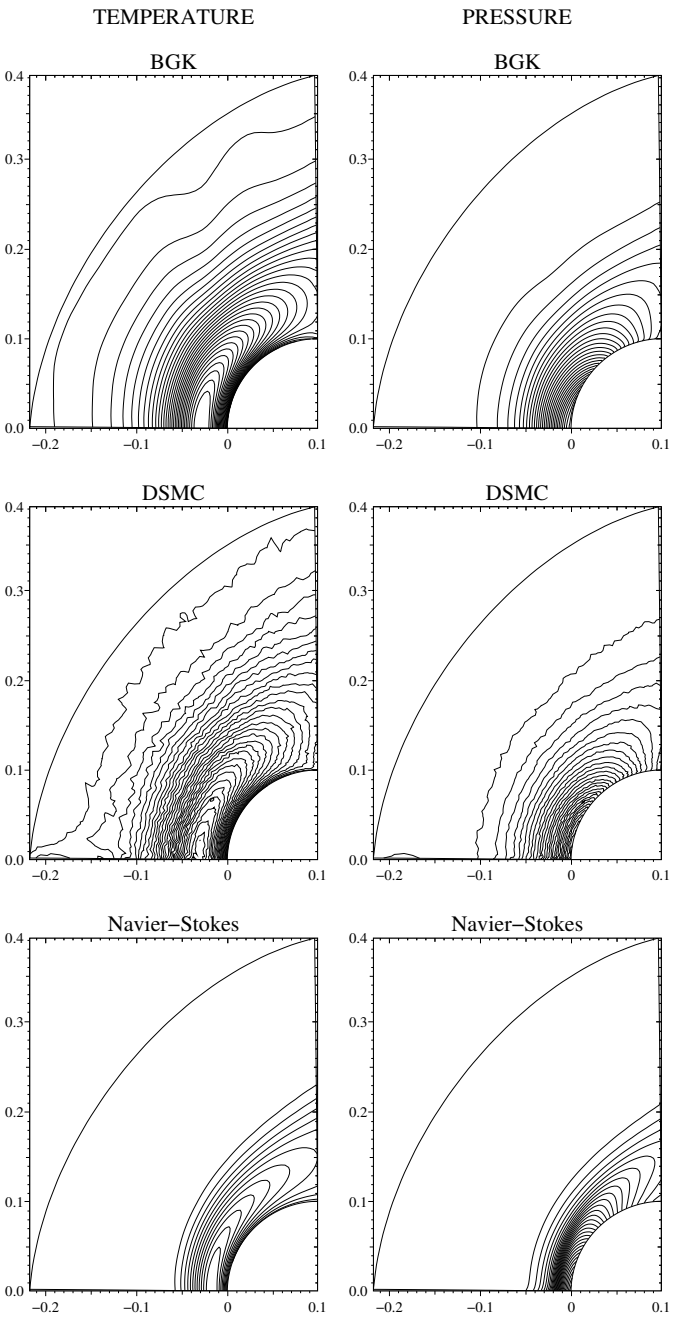

FIG. 11. Axisymmetric flow past a sphere. Temperature and pressure contours for BGK, DSMC, and Navier-Stokes.

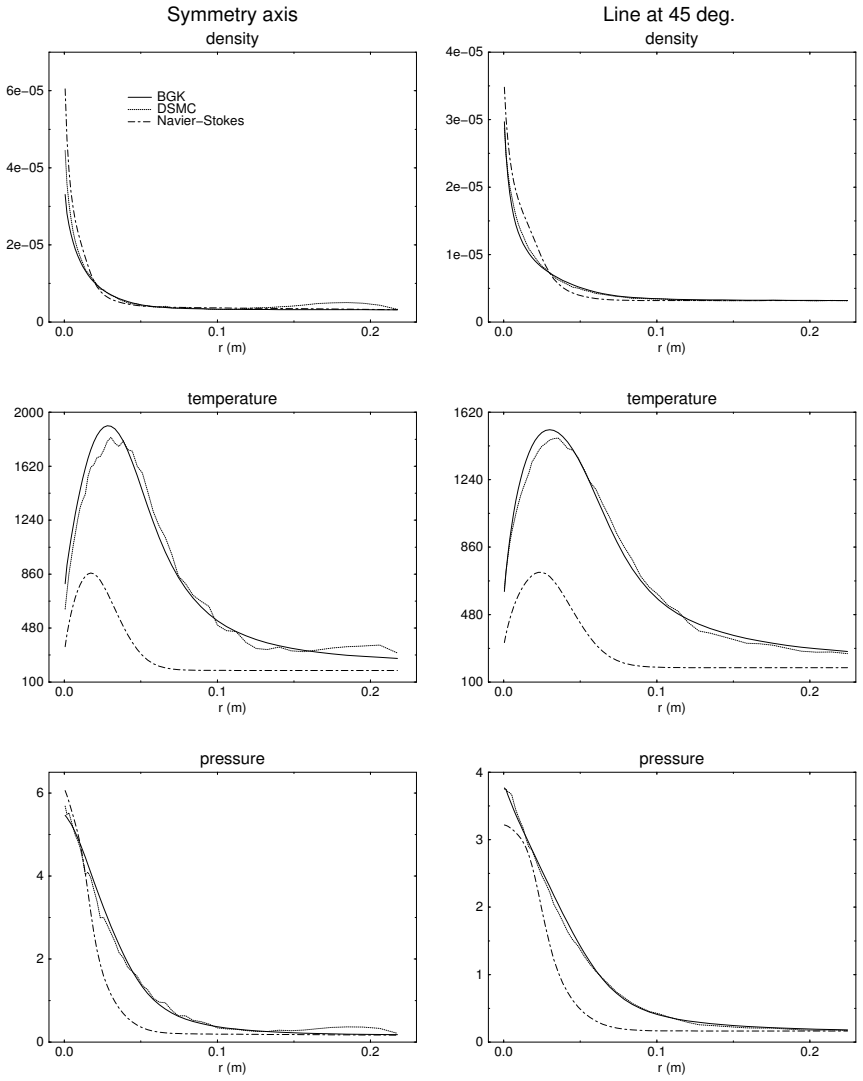

FIG. 12. Axisymmetric flow past a sphere. Density, temperature, and pressure profiles as functions of r along the symmetry axis and a line at 45°.

7. CONCLUSION

We have presented a new numerical method for BGK and BGK-ES equations. It is based on discrete-velocity models for the collision and transport operators, for plane and axisymmetric geometries, and on a linearized implicit scheme. Our discrete-velocity models satisfy important mathematical properties (conservation and entropy). They permit us to have robust algorithms that do not require a fine velocity grid. Whereas these properties are not a necessary condition for high accuracy, they make it possible to yield plausible results even with low-resolution velocity grids.

Our numerical results have been compared to the DSMC reference method. They have been noted to be very closed to DSMC results for transitional flows, with a comparable CPU time. The BGK equation is a simplified model, but here it appears sufficient for these flows, and the BGK-ES model allows for more physics. We have proved that our deterministic method is well suited for situations - like recirculation flows - where the DSMC method may be difficult to use. Our study on axisymmetric transport operator allows to make simulations on 3D geometries with axial symmetry.

Moreover, due to the linear complexity of our algorithms, our method may be extended to 3D non axisymmetric computations, without a prohibitive increasing of the computational cost. The explicit and implicit schemes of sections 5.1 and 5.2 can be extended with the same properties. The only difference is that the blocks of the transport matrix T (see figure 1) would be heptadiagonal instead of pentadiagonal. Thus the Gauss-Seidel method proposed in section 5.2.2 to split the matrix T should be modified.

Finally, we mention that an extension of our method to polyatomic gases is in preparation.

ACKNOWLEDGMENT

I thank P. Charrier and B. Dubroca for their encouragements and for numerous discussions that have been very helpful.

REFERENCES

1. P. Andriès, J.-F. Bourgat, P. Le Tallec, and B. Perthame. Etude de modèles d'énergie interne BGK pour le calcul d'écoulements raréfiés. Technical report, INRIA, 1998.
2. P. Andriès, P. Le Tallec, J.-P. Perlat, and B. Perthame. The Gaussian-BGK Model of Boltzmann Equation with Small Prandtl Number. preprint.
3. K. Aoki, K. Kanba, and S. Takata. Numerical Analysis of a Supersonic Rarefied Gas Flow Past a Flat Plate. *Phys. Fluids*, 9(4), 1997.
4. H. Babovski. Discretization and Numerical Schemes for Steady Kinetic Model Equations. *Computers Math. Applic.*, 35(1/2):29–40, 1998.
5. P.L. Bathnagar, E.P. Gross, and M. Krook. A model for collision processes in gases. I. small amplitude processes in charged and neutral one-component systems. *Phys. Rev.*, 94:511–525, 1954.
6. D. Bergers. Kinetic model solution for axisymmetric flow by the method of discrete ordinates. *J. Comput. Phys.*, 57:285–302, 1985.
7. G.A. Bird. *Molecular Gas Dynamics and the Direct Simulation of Gas Flows.* Oxford Science Publications, 1994.
8. A.V. Bobylev and J. Struckmeier. Implicit and iterative methods for the Boltzmann equation. *Transp. Th. Stat. Phys.*, 25(2):175–195, 1996.

9. F. Bouchut and B. Perthame. A BGK model for small Prandtl number in the Navier-Stokes approximation. *Journal Stat. Physics*, 71(1-2):191–207, 1993.
10. J.-F. Bourgat, P. Le Tallec, and M. D. Tidriri. Coupling Boltzmann and Navier-Stokes equations by friction. *J. Comput. Phys*, 127:227–245, 1996.
11. C. Buet. A Discrete-Velocity Scheme for the Boltzmann Operator of Rarefied Gas Dynamics. *Transp. Th. Stat. Phys.*, 25(1):33–60, 1996.
12. R. E. Caflisch, S. Jin, and G. Russo. Uniformly accurate schemes for hyperbolic systems with relaxation. *SIAM J. Numer. Anal.*, 34:246, 1997.
13. C. Cercignani. *The Boltzmann Equation and Its Applications*, volume 68. Springer-Verlag, Lectures Series in Mathematics, 1988.
14. S. Chapman and T.G. Cowling. *The Mathematical Theory of Non-Uniform Gases*. Cambridge University Press, 1970.
15. P. Charrier, B. Dubroca, J.-L. Feugeas, and L. Mieussens. Discrete-velocity models for kinetic nonequilibrium flows. *C.R Acad. Sci.*, Serie I, 326(11):1347–1352, june 1998. Paris.
16. P. Degond and B. Lucquin-Desreux. An entropy scheme for the Fokker-Planck collision operator of plasma kinetic theory. *Numer. Math.*, 68:239–262, 1994.
17. E. Gabetta, L. Pareschi, and G. Toscani. Relaxation Schemes for Non Linear Kinetic Equations. *SIAM J. Numer. Anal.*, 34(6):2168–2194, 1997.
18. V. Garzó and A. Santos. Comparison Between the Boltzmann and BGK Equations for Uniform Shear Flows. *Physica A*, 213:426–434, 1995.
19. L. H. Holway. Kinetic theory of shock structure using an ellipsoidal distribution function. In New York Academic Press, editor, *Rarefied Gas Dynamics, Vol. 1 (Proc. Fourth Internat. Sympos. Univ. Toronto, 1964)*, pages 193–215, 1966.
20. D. Issautier. Convergence of a Weighted Particle Method for Solving The Boltzmann (B.G.K.) Equation. *SIAM J. Numer. Anal.*, 33(6):2099–2119, 1996.
21. S. Jin and C. D. Levermore. Numerical schemes for hyperbolic conservation laws with stiff relaxation terms. *J. Comput. Phys.*, 126:449, 1996.
22. I. N. Larina and V. A. Rykov. A Numerical Method for Calculating Axisymmetric Rarefied Gas Flows. *Comp. Maths. math. Phys*, 38(8):1391–1403, 1998.
23. J.-C. Lengrand. Mise en oeuvre de la méthode de Monte Carlo pour la simulation numérique d'un écoulement de gaz raréfié. Technical report, CNRS, 1986. RC 86-4.
24. G. Liu. A method for constructing a model for the Boltzmann equation. *Phys; Fluids A*, 2, 1990.
25. L. Mieussens. Convergence of a discrete-velocity model for the Boltzmann-BGK equation. *C.R Acad. Sci.*, Serie I(328):1231–1236, 1999, and *Computers Math. Applic.*, 2000, in press.
26. L. Mieussens. Discrete Velocity Model and Implicit Scheme for the BGK Equation of Rarefied Gas Dynamics. *Math. Models and Meth. in Applied Sciences*, 2000, in press.
27. T. Ohwada. Higher order approximation methods for the Boltzmann equation. *J. Comput. Phys.*, 139:1–14, 1998.
28. L. Pareschi and R. E. Caflisch. An implicit Monte Carlo method for Rarefied Gas Dynamics. *J. Comput. Phys.*, 154:90–116, 1999.
29. B. Perthame. Global existence to the BGK model of Boltzmann Equation. *J. Diff. Eq.*, 82:191–205, 1989.
30. F. Rogier and J. Schneider. A Direct Method For Solving the Boltzmann Equation. *Transp. Th. Stat. Phys.*, 23(1-3):313–338, 1994.
31. Y. M. Shakhov. The Axisymmetric Non-Linear Steady Flow of a Rarefied Gas in a Pipe of Circular Cross-Section. *Comp. Maths and Math. Phys*, 36(8):1123–1131, 1996.
32. Ye. M. Shakhov. The Two-dimensional Non-linear Problem of the Motion of a Rarefied Gas Between Two Parallel Plates. *Zh. Vychisl. Mat. Mat. Fiz.*, 35:83–94, 1994.
33. Y. Sone, S. Takata, and H. Sugimoto. The behavior of a gas in the continuum limit in the light of kinetic theory: the case of cylindrical couette flows with evaporation and condensation. *Phys. Fluids*, 8(12), 1996.
34. H. Struchtrup. The BGK-Model with Velocity-Dependent Collision Frequency. *Continuum Mech. Thermodyn.*, 9:23–31, 1997.

35. H. Sugimoto and Y. Sone. Numerical analysis of steady flows of a gas evaporating from its cylindrical condensed phase on the basis of kinetic theory. *Phys. Fluids A*, 4(2), 1992.

36. J.Y. Yang and J.C. Huang. Rarefied Flow Computations Using Nonlinear Model Boltzmann Equations. *Journal of Computational Physics*, 120:323–339, 1995.

37. H. C. Yee. *A Class of High-Resolution Explicit and Implicit Shock-Capturing Methods*. von Karman Institute for Fluid Dynamics, Lectures Series, n^{o}4. 1989.